Precision Engineering 85 (2024) 72–88

Contents lists available at ScienceDirect

Precision Engineering

journal homepage: www.elsevier.com/locate/precision

Workshop-suited identification of thermo-elastic errors of three-axis machine tools using on-machine measurement☆

André Breitzke *, Wolfgang Hintze

Institute of Production Management and Technology, Hamburg University of Technology, Hamburg, Germany

ARTICLE INFO

Keywords:
Machine tool
Thermo-elastic errors
Identification
On-machine measurement

ABSTRACT

This paper presents a method for workshop-suited identification of thermo-elastic errors of three-axis machine tools (MTs) using on-machine measurement. For this purpose, a new design for a three dimensional artifact is presented. Using the artifact, it is possible to identify all relevant geometric errors of three-axis portal milling machines in table design. The method presented is therefore suitable for the one-time identification of geometric errors caused by manufacturing inaccuracies, assembly-related deviations and wear, and for the identification of thermally induced geometry errors over a long-term period. Since the artifact is scalable in size, it can be easily adapted to different machine sizes. The presented method thus represents a universal and inexpensive possibility to measure geometric and especially thermo-elastic errors.

Within the scope of this paper, an error model was established for the investigated machine type and an artifact design was derived on the basis of this model. The suitability of the artifact for identifying thermo-elastic errors has also been investigated experimentally. For this purpose, an artifact made of thermo-invariant material (Invar) was produced. This artifact was measured cyclically on a MT with three linear axes, which was exposed to a controlled thermal load in a temperature chamber. The positions of the geometric features were collected using a 3D touch trigger probe. In addition, the ambient temperatures were recorded. The results of this measurement are discussed in this paper.

1. Introduction

In the course of technical progress and globalized competition, technical products are becoming more and more diverse and complex. As a result, the demands on industrial production are constantly increasing. Particularly important in this context is the ability to produce high accurate parts. This leads to the demand for machine tools (MTs) with the highest possible machining accuracies [1]. Ensuring high machining accuracies is thus a key competitive advantage for MT manufacturers.

The achievable machining accuracies could be steadily increased in the past [2]. The progress achieved in this field is essentially based on improvements in geometric, static and dynamic machine behavior. The thermo-elastic machine behavior, on the other hand, is not yet sufficiently mastered [3]. This leads to the fact that today up to 75 % of the deviations occurring on the workpiece are due to thermo-elastically caused errors [4]. The understanding and mastering of thermo-elastic machine behavior is therefore one of the greatest challenges in MT development [3].

The issue of thermo-elastic machine behavior has been intensively investigated in the last decades. As a result, there is a considerable number of different approaches for optimizing thermo-elastic machine behavior in science and industry. These include design principles, temperature control strategies and model- as well as data-based correction approaches [4]. A key challenge for all approaches is the measurement and appropriate description of thermo-elastic errors. The measurement is usually closely linked to the measurement of geometric errors, since thermo-elastic errors are considered as a transient component of corresponding static geometric errors [5]. Therefore, in principle, any measuring device suitable for measuring geometric errors can be used, whereby the measuring time must be sufficiently short so that transient thermo-elastic displacements during the measurement only have a negligible influence on the measurement result [6].

Schwenke et al. [7], Kwasny et al. [8] and Ibaraki and Knapp [9] give comprehensive overviews of the methods used to measure geometric errors. These methods can be divided into direct and indirect measurement methods. Schwenke et al. [7] categorize direct methods as the measurement of errors of a single moving axis. Indirect methods, on the other hand, process signals consisting of superposed errors that occur during multi-axis movements.

☆ This paper was recommended by Associate editor Prof. R. Leach.

* Corresponding author.
E-mail addresses: andre.breitzke@tuhh.de (A. Breitzke), w.hintze@tuhh.de (W. Hintze).

https://doi.org/10.1016/j.precisioneng.2023.09.009
Received 7 February 2023; Received in revised form 14 September 2023; Accepted 25 September 2023
Available online 26 September 2023

Direct measurements, such as measuring mandrels and angles according to ISO 230-3:2020 [10], straightedges, line scales, step gauges or laser interferometers, have the disadvantage that only specific geometric errors can be measured. In some cases, more geometric errors can be measured with these methods when the measuring instruments are reconfigured. However, this is not possible for the measurement of thermo-elastic errors, because the thermal situation of the machine changes during the assembly time [6]. Brecher et al. [5] overcomes this disadvantage by using a measurement setup consisting of a laser beam directed by pentaprisms and position sensitive detectors (PSD), whereby the approach can be classified at the junction between direct and indirect measurements. With this setup it is possible to detect 13 of 21 geometric errors of the three linear axes of a 3-axis MT.

Alternatively, indirect measurement methods are used. These primarily include dimensional artifacts and displacement measurements, such as ball bar [11] and lasertracer [12]. Dimensional artifacts offer a cost-effective and workshop-suitable possibility to measure geometric errors for small and medium-sized MTs [13,14]. Carmignato et al. [14] provides an overview of dimensional artifacts and discusses their characteristics and role in supporting production. Wennemer [6] addresses suitability of artifacts for measuring thermo-elastic errors. Summarizing these publications, there are currently, on the one hand, dimensional artifacts with which all 21 geometric errors of the three linear axes of 3-axis MTs can be determined according to ISO 230-1:2012 [13,15–17], and, on the other hand, artifacts which are suitable for the determination of thermo-elastic errors due to unnecessary setup modifications and short measuring times [18–22]. However, there is a gap in research for artifacts that measure all 21 geometric errors of the three linear axes of 3-axis MTs in one setup and thus are suitable for the detection of thermo-elastic errors. In this paper, a dimensional artifact is presented to fill this research gap.

The artifact presented in this paper is based on the work of Breitzke and Hintze on workshop-suited geometric errors identification of three-axis MTs [23]. This paper addresses an improvement of the artifact presented in [23] and shows a new artifact design that can measure all relevant geometric errors in one setup. On the one hand, this new artifact can be used to test the geometry of a 3-axis MT as described in [23] in a fast, accurate, cost-effective way. On the other hand, it is possible to investigate thermo-elastic errors, although the investigation of the influence of internal heat sources is limited, since it is not possible to measure positions and move the axes or operate the motor spindle at the same time. In this paper, the focus lies on the investigation of thermo-elastic errors. For this purpose, a 3-axis MT is examined in a temperature chamber with the help of the presented artifact.

The paper is structured as follows. At the beginning, geometric machine errors are explained in general. In the same section, a kinematic error model is established for the MT investigated in this paper (see Section 2). With this knowledge, the next section derives a dimensional artifact that can be used to measure all errors according to the error model (see Section 3). Subsequently, the identification of geometric errors with the artifact is explained (see Section 4). That section explains the measurement process and the evaluation of the measurement data. In the next section, the artifact is applied experimentally by measuring the geometric errors of a MT under ambient thermal load to show a typical use case (see Section 5). For this purpose, a MT is placed in a temperature chamber and exposed to a defined change in ambient temperature. Finally, the results of the experimental investigation and the suitability of the artifact for the identification of thermo-elastic errors are discussed (see Section 6).

2. Modeling of geometric errors of 3-axis portal milling machines in table design

In this section, geometric errors of MTs are explained in general. In this context, the notation of errors is also introduced, as it will be used in the later sections. Afterwards, an error model for a 3-axis MT is derived.

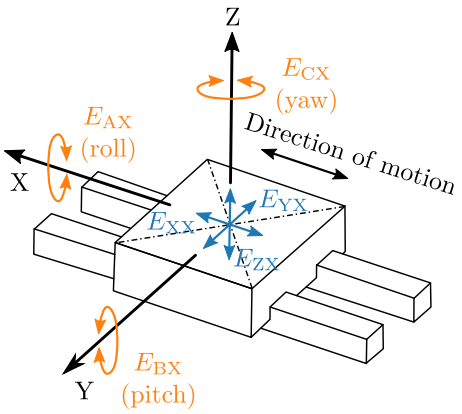

Fig. 1. Component errors of a linear X-axis [15].

Table 1
Component errors of the three linear axes of 3-axis MTs [15].

Dir.	Component errors		
	X-axis	Y-axis	Z-Axis
X	E_{XX} (positioning)	E_{XY} (straightness)	E_{XZ} (straightness)
Y	E_{YX} (straightness)	E_{YY} (positioning)	E_{YZ} (straightness)
Z	E_{ZX} (straightness)	E_{ZY} (straightness)	E_{ZZ} (positioning)
A	E_{AX} (roll)	E_{AY} (yaw)	E_{AZ} (tilt around X)
B	E_{BX} (pitch)	E_{BY} (roll)	E_{BZ} (tilt around Y)
C	E_{CX} (yaw)	E_{CY} (pitch)	E_{CZ} (roll)

2.1. Description of geometric errors

To describe the geometric errors of MTs, a rigid-body behavior of the machine is assumed [2,7,15,24,25]. The errors are divided into component errors and position errors. Component errors describe the errors of a moving component. Each component can have six component errors according to its number of degrees of freedom [26]. As an example, the component errors of a linear X-axis are shown in Fig. 1. The component errors of the three linear axes of a MT with three linear axes and their notation can be found in Table 1.

Location errors of a linear axis are defined as the deviation from the nominal position and orientation of the axis in the machine coordinate system [7]. A linear axis has three location errors: Two orientation errors and the zero position. As an example, the location errors of a linear X-axis are shown in Fig. 2. The three linear axes of 3-axis MT have nine location errors (see also Table 2). Six of these nine location errors do not have to be taken into account because they define the coordinate system of the MT. E_{X0X}, E_{Y0Y} and E_{Z0Z} define the zero point of the coordinate system. Depending on the choice of reference axes, the MT coordinate system can be defined in different ways. A common variant is as follows: E_{B0X} and E_{C0X} define the X-axis and E_{A0Y} the Y-axis of the MT coordinate system. Therefore only E_{C0Y}, E_{A0Z} and E_{B0Z} need to be considered.

2.2. Kinematic error model

In this paper, a kinematic error model is established for a 3-axis portal milling machine in table design. In the considered MT, the machine table moves with the workpiece. The machine configuration is thus in accordance with ISO 10791-2 V [w X' b Y Z (C) t]. This is also

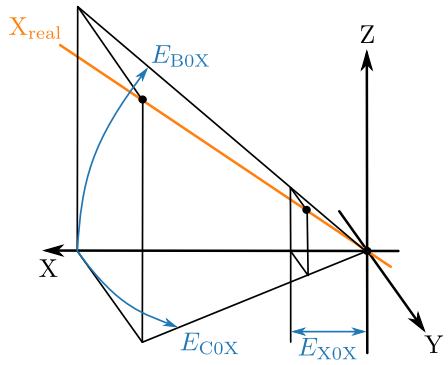

Fig. 2. Location errors of a linear X-axis.

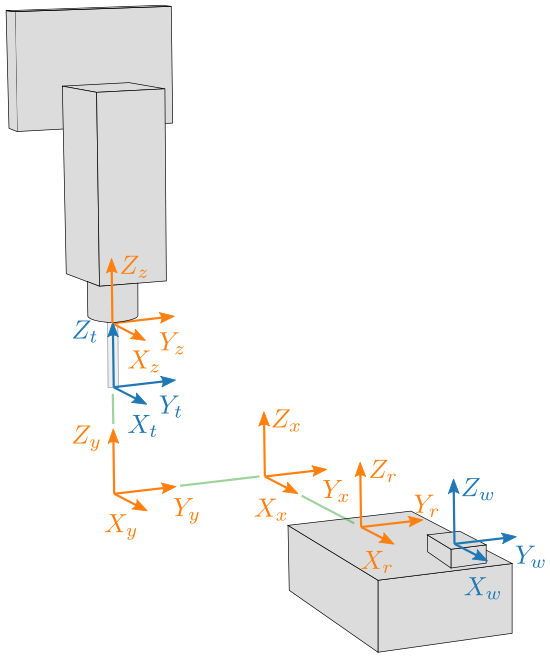

Fig. 3. Kinematics for error model and axis configuration of the MT.

Table 2
Location errors of the three linear axes of 3-axis MTs [15].

Dir.	Location errors		
	X-axis	Y-axis	Z-Axis
X	E_{X0X} (zero position)	–	–
Y	–	E_{Y0Y} (zero position)	–
Z	–	–	E_{Z0Z} (zero position)
A	–	E_{A0Y} (squareness)	E_{A0Z} (squareness)
B	E_{B0X} (squareness)	–	E_{B0Z} (squareness)
C	E_{C0X} (squareness)	E_{C0Y} (squareness)	–

the configuration of the MT used for the investigations in Section 5. However, in order to simplify the kinematic error model, the machine will be considered in the following derivation as if the machine table were fixed and the tool moved around the workpiece.

For the kinematic model, a rigid-body approach is chosen, i.e. the individual components of the machine are considered to be ideally rigid. In addition, it is assumed that the errors of the individual components are decoupled from each other. These simplifications are generally used because the scope of measurement would otherwise be very large [2,19,24,27–38]. Homogeneous coordinates are used to derive the kinematic model [39]. Six coordinate systems are introduced: The Workpiece coordinate system (O_w, X_w, Y_w, Z_w), the reference coordinate system (O_r, X_r, Y_r, Z_r), the X-axis coordinate system (O_x, X_x, Y_x, Z_x), the Y-axis coordinate system (O_y, X_y, Y_y, Z_y), the Z-axis coordinate system (O_z, X_z, Y_z, Z_z) and the tool coordinate system (O_t, X_t, Y_t, Z_t). The reference coordinate system is located on the center of the machine table and is fixed to it. The workpiece coordinate system can be defined by the user as desired (usually a position on the workpiece is selected) and has an offset w_x, w_y, w_z relative to the reference coordinate system. The X-axis coordinate system describes the X-movement of the portal relative to the reference coordinate system. The Y-axis coordinate system describes the Y-movement of the Y-table relative to the reference coordinate system. The Z-axis coordinate system describes the Z-movement of the spindle relative to the reference coordinate system. The tool coordinate system describes the position of the tool tip and has a Z-offset t_z relative to the Z-axis coordinate system. The errors of the motor spindle are not considered in this paper, as it is assumed that the machine is a high-precision milling machine, for which geometric errors are minor in comparison.

To derive the error model, the transformation of any point from the workpiece coordinate system to the tool coordinate system is considered for the ideal and the real machine. The differences between the ideal and the real transformation result in the geometric errors.

An arbitrary position in the workpiece coordinate system is described by the vector

$$\boldsymbol{p}^w = \begin{bmatrix} p_x^w & p_y^w & p_z^w & 1 \end{bmatrix}^T. \tag{1}$$

To describe the vector $\boldsymbol{p}^w$ in the tool coordinate system, a kinematic chain can be used as follows:

$$\begin{aligned} \boldsymbol{p}^t &= \boldsymbol{T}_z^t\, \boldsymbol{T}_y^z\, \boldsymbol{T}_x^y\, \boldsymbol{T}_r^x\, \boldsymbol{T}_w^r\, \boldsymbol{p}^w \\ &= \underbrace{(\boldsymbol{T}_t^z)^{-1}\, (\boldsymbol{T}_z^y)^{-1}\, (\boldsymbol{T}_y^x)^{-1}\, (\boldsymbol{T}_x^r)^{-1}\, \boldsymbol{T}_w^r}_{\boldsymbol{T}_w^t}\, \boldsymbol{p}^w \end{aligned} \tag{2}$$

where $\boldsymbol{T}_i^j$ represents the homogeneous transformation matrix that transforms a vector $\boldsymbol{p}^i$ described in the coordinate system i into the description of the vector $\boldsymbol{p}^j$ in the coordinate system j. The transformation matrices for the ideal and the real machine are listed in the appendix (see Appendices A.1 and A.2).

In Section 2.1 it was described that the zero position does not have to be considered as a location error because it defines the coordinate system. However, a typical thermo-elastic machine behavior is a zero displacement. Therefore, the errors E_{X0X}, E_{Y0Y} and E_{Z0Z} will be included in the kinematic model. In this way, they represent the change of the zero position with respect to a defined reference state of the MT. Accordingly, these errors are equal to zero for the one-time determination of the geometric errors.

To calculate the geometric errors, the vector $\boldsymbol{p}^w$ is transformed from the workpiece coordinate system to the tool coordinate system using the ideal transformation matrix $\boldsymbol{T}_{w,ideal}^t$ and the real transformation matrix $\boldsymbol{T}_{w,real}^t$. The error vector $\boldsymbol{e}$ is defined as the difference of the resulting vectors

$$\begin{aligned} \boldsymbol{e} &= \begin{bmatrix} \Delta x & \Delta y & \Delta z & 1 \end{bmatrix}^T \\ &= \boldsymbol{T}_{w,real}^t\, \boldsymbol{p}^w - \boldsymbol{T}_{w,ideal}^t\, \boldsymbol{p}^w \\ &= \underbrace{[\boldsymbol{T}_{w,real}^t - \boldsymbol{T}_{w,ideal}^t]}_{\boldsymbol{E}}\, \boldsymbol{p}^w, \end{aligned} \tag{3}$$

where E is the error matrix.

The errors of the individual axes result in:

$$\begin{aligned}\Delta x =& x_{real} - x_{ideal}\\ =& - E_{XX}(x) - E_{XY}(y) - E_{XZ}(z)\\ & - E_{C0Y}y - E_{B0Z}z\\ & + E_{BX}(x)\left(-p_z^w - w_z\right)\\ & + E_{CX}(x)\left(p_y^w + w_y\right)\\ & + E_{BY}(y)\left(-p_z^w - w_z\right)\\ & + E_{CY}(y)\left(p_y^w + w_y - y\right)\\ & + E_{BZ}(z)\left(-p_z^w - w_z + z\right)\\ & + E_{CZ}(z)\left(p_y^w + w_y - y\right)\\ & - E_{X0X}\end{aligned} \tag{4}$$

$$\begin{aligned}\Delta y =& y_{real} - y_{ideal}\\ =& - E_{YX}(x) - E_{YY}(y) - E_{YZ}(z)\\ & - E_{A0Z}z\\ & + E_{AX}(x)\left(p_z^w + w_z\right)\\ & + E_{CX}(x)\left(-p_x^w - w_x + x\right)\\ & + E_{AY}(y)\left(p_z^w + w_z\right)\\ & + E_{CY}(y)\left(-p_x^w - w_x + x\right)\\ & + E_{AZ}(z)\left(p_z^w + w_z - z\right)\\ & + E_{CZ}(z)\left(-p_x^w - w_x + x\right)\\ & - E_{Y0Y}\end{aligned} \tag{5}$$

$$\begin{aligned}\Delta z =& z_{real} - z_{ideal}\\ =& - E_{ZX}(x) - E_{ZY}(y) - E_{ZZ}(z)\\ & + E_{AX}(x)\left(-p_y^w - w_y\right)\\ & + E_{AY}(y)\left(-p_y^w - w_y + y\right)\\ & + E_{AZ}(z)\left(-p_y^w - w_y + y\right)\\ & + E_{BX}(x)\left(p_x^w + w_x - x\right)\\ & + E_{BY}(y)\left(p_x^w + w_x - x\right)\\ & + E_{BZ}(z)\left(p_x^w + w_x - x\right)\\ & - E_{Z0Z}\end{aligned} \tag{6}$$

Only the contact point between the workpiece and the tool is relevant for the geometric errors. In order to approach a point $\boldsymbol{p}$ with the tool tip, $\boldsymbol{p}^t$ must correspond to the zero vector

$$\boldsymbol{p}^t = \begin{bmatrix}0 & 0 & 0 & 1\end{bmatrix}^T, \tag{7}$$

since the origin of the tool coordinate system is located at the tool tip. Using the ideal transformation, we can then derive the following relationships:

$$\begin{aligned}x =& p_x^w + w_x\\ y =& p_y^w + w_y\\ t_z + z =& p_z^w + w_z\end{aligned} \tag{8}$$

With these relationships, Eq. (4) to (6) simplify to

$$\begin{aligned}\Delta x =& x_{real} - x_{ideal}\\ =& - E_{XX}(x) - E_{XY}(y) - E_{XZ}(z)\\ & - E_{C0Y}y - E_{B0Z}z\\ & - E_{BX}(x)\left(t_z + z\right) + E_{CX}(x)y\\ & - E_{BY}(y)\left(t_z + z\right)\\ & - E_{BZ}(z)t_z - E_{X0X}\end{aligned} \tag{9}$$

$$\begin{aligned}\Delta y =& y_{real} - y_{ideal}\\ =& - E_{YX}(x) - E_{YY}(y) - E_{YZ}(z)\\ & - E_{A0Z}z + E_{AX}(x)\left(t_z + z\right)\\ & + E_{AY}(y)\left(t_z + z\right) + E_{AZ}(z)t_z\\ & - E_{Y0Y}\end{aligned} \tag{10}$$

$$\begin{aligned}\Delta z =& z_{real} - z_{ideal}\\ =& - E_{ZX}(x) - E_{ZY}(y) - E_{ZZ}(z)\\ & - E_{AX}(x)y - E_{Z0Z}\end{aligned} \tag{11}$$

In this way, the errors are only dependent on the machine coordinates x, y and z as well as the offset t_z, which results from the tool length.

For further simplification, it is assumed that the lengths of the tools are constant:

$$t_z = const. \tag{12}$$

It is also assumed that the tool diameter is small. These assumptions can be made in the context of investigating the thermal behavior of a MT with a 3D touch trigger probe. With these assumptions, the Z-axis tilt error around the X-axis $E_{AZ}(z)$ and the Z-axis tilt error around the Y-axis $E_{BZ}(z)$ can be neglected.

This is because both errors can be corrected by the straightness error and the squareness error of the Z-axis. Thus:

$$E_{AZ}(z) = 0 \tag{13}$$

$$E_{BZ}(z) = 0 \tag{14}$$

This simplifies Eqs. (9)–(11) to:

$$\begin{aligned}\Delta x =& x_{real} - x_{ideal}\\ =& - E_{XX}(x) - E_{XY}(y) - E_{XZ}(z)\\ & - E_{C0Y}\cdot y - E_{B0Z}\cdot z\\ & - \left[E_{BX}(x) + E_{BY}(y)\right]\left(t_z + z\right)\\ & + E_{CX(x)}\cdot y - E_{X0X}\end{aligned} \tag{15}$$

$$\begin{aligned}\Delta y =& y_{real} - y_{ideal}\\ =& - E_{YX}(x) - E_{YY}(y) - E_{YZ}(z)\\ & + \left[E_{AX}(x) + E_{AY}(y)\right]\left(t_z + z\right)\\ & - E_{A0Z}\cdot z - E_{Y0Y}\end{aligned} \tag{16}$$

$$\begin{aligned}\Delta z =& z_{real} - z_{ideal}\\ =& - E_{ZX}(x) - E_{ZY}(y) - E_{ZZ}(z)\\ & - E_{AX}(x)\cdot y - E_{Z0Z}\end{aligned} \tag{17}$$

The Eqs. (15), (16) and (17) establish a relationship between the machine position x, y, z and the deviations in each axis Δx, Δy, Δz. Using these equations, an artifact design is derived in the next section, which can be used to determine the individual error components.

3. Artifact design

The aim of the design of the artifact is to provide a method for the measurement of geometric errors of machine tools that can capture all relevant geometric errors and can be carried out periodically to evaluate the long-term behavior. In particular, the measurement of all relevant geometric errors over a long period of time represents a unique selling point and opens up various application scenarios. One main area of use is the possibility of evaluating the change of geometric errors under thermal load. This will be the main focus of this paper. The derivation of the artifact geometry is described below.

3.1. Derivation of the artifact geometry

Based on common MT calibration artifacts such as step gauges [2, 40] and hole plates [41–44], a 3D artifact is developed to measure all relevant geometric errors of the three linear axes of 3-axis MTs according to ISO 10791-2 V [w X' b Y Z (C) t]. The errors of the motor spindle are not taken into account here. For this purpose, geometric features of the artifact are derived from the Eqs. (15), (16) and (17), which allow the measurement of the different errors in one setup.

3.1.1. Derivation of geometric features for positioning and straightness errors of the X-axis

The X-positioning error E_{XX} can be calculated from Eq. (15):

$$\begin{aligned}\Delta x_i =& x_{i,actual} - x_{i,nominal}\\ =& - E_{XX}(x_i) - E_{XY}(y_i) - E_{XZ}(z_i)\\ & - E_{C0Y}\cdot y_i - E_{B0Z}\cdot z_i\\ & - \left[E_{BX}(x_i) + E_{BY}(y_i)\right](t_z + z_i)\\ & + E_{CX}(x_i)\cdot y_i - E_{X0X}\end{aligned} \tag{18}$$

Accordingly, i geometric features must be available in the X-direction at which the X-differences Δx_i can be determined. In order for the X-positioning error E_{XX} to be determined independently of other error factors, the Y- and Z-positions y_i and z_i of the features must be identical. Therefore, the following simplifications are valid:

$$z_i + t_z = z_{m,1} = const. \tag{19}$$

$$y_i = y_{m,1} = const. \tag{20}$$

$$E_{XY}(y_i) = const. \tag{21}$$

$$E_{XZ}(z_i) = const. \tag{22}$$

$$E_{C0Y}\cdot y_i = const. \tag{23}$$

$$E_{B0Z}\cdot z_i = const. \tag{24}$$

$$E_{BY}(y_i) = const. \tag{25}$$

$$E_{X0X} = const. \tag{26}$$

With these simplifications, Eq. (15) results in

$$\begin{aligned}\Delta x_i =& - E_{XX}(x_i) - E_{BX}(x_i)\cdot z_{m,1}\\ & + E_{CX}(x_i)\cdot y_{m,1} + C_1\end{aligned} \tag{27}$$

where $y_{m,1}$ and $z_{m,1}$ is the measurement position and C_1 is a constant. Furthermore, it is defined that the X-error due to the pitch error of the X-axis $E_{BX}(x_i)$ at the Z-position $z_{m,1}$ is zero, i.e. the error is completely attributed to the X-positioning error at this position. It is also defined that the X-error due to the yaw error of the X-axis $E_{CX}(x_i)$ at the Y-position $y_{m,1}$ is zero, i.e. the error is completely assigned to the X-positioning error at this position. Thus it follows:

$$\Delta x_i = -E_{XX}(x_i) + C_1 \tag{28}$$

This can be used to determine the positioning error of the X-axis E_{XX} at the positions x_i by comparing the measured positions $x_{i,actual}$ with the nominal positions $X_{i,nominal}$:

$$\begin{aligned}E_{XX}(X_i) &= -\Delta X_i + C_1\\ &= X_{i,nominal} - X_{i,actual} + C_1\end{aligned} \tag{29}$$

The constant C_1 can be specified by appropriate conditions, such as $E_{XX}(x) = 0$ for $x = 0$. These considerations lead to the fact that geometric features in the X-direction with identical Y- and Z-positions must be available for the artifact, whose Y- and Z-positions can be determined.

The geometric features required to determine the straightness errors of the X-axis in the Y- and Z-directions E_{YX} and E_{ZX} can be derived in the same way. For these errors, there must be geometric features in the X-direction with identical Y- and Z-positions, whose Y- and Z-positions can be determined. The exact type of geometric features is irrelevant. These can be, for example, steps, holes or spheres whose positions can be measured with a probe. When holes are used, as shown in the figures in this section, there must be a surface in or next to the holes where the Z position can be measured. An example where holes have been used is shown in Fig. 4.

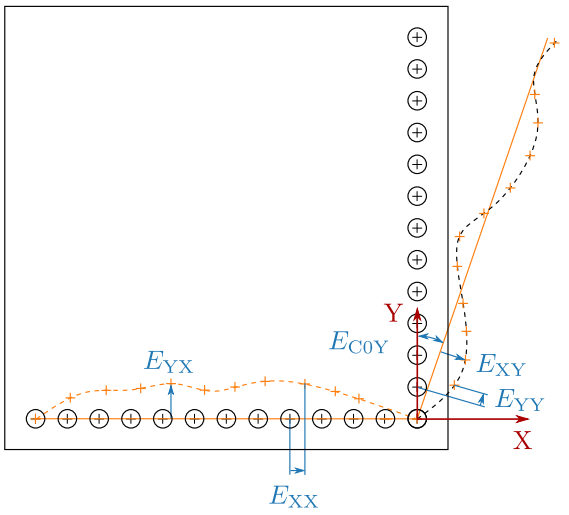

Fig. 4. Exemplary arrangement of holes on a plate for determining the position, straightness and squareness errors of the X- and Y-axis [23]. Black plus signs are nominal positions; orange plus signs are measurement points; blue arrows indicate geometric errors; red arrows represent the coordinate system. (For interpretation of the references to color in this figure legend, the reader is referred to the web version of this article.)

The straightness errors of the X-axis in the Y- and Z-directions E_{YX} and E_{ZX} are evaluated relative to the orientation of the coordinate system, which can be defined (see Section 4.1, step 2).

For the derivation of the further geometric features, it can be taken into account that the errors E_{XX}, E_{YX} and E_{ZX} are determined after the measurement of these features and can be assumed as known for the further considerations. This simplifies the search for further geometric features.

3.1.2. Derivation of geometric features for positioning and straightness errors of the Y-axis as well as for the perpendicularity error between the X- and Y-axis

The geometric features for determining the positioning and straightness errors of the Y-axis can basically be derived in the same way as for the X-axis. In the following, therefore, only the derivation of the features for the straightness error of the Y-axis in the X-direction E_{XY} and the perpendicularity error from the Y- to the X-axis E_{C0Y} is shown, since this derivation is slightly different.

The errors E_{XY} and E_{C0Y} can be calculated using Eq. (15):

$$\begin{aligned}\Delta x_i =& x_{i,actual} - x_{i,nominal}\\ =& - E_{XX}(x_i) - E_{XY}(y_i) - E_{XZ}(z_i)\\ & - E_{C0Y}\cdot y_i - E_{B0Z}\cdot z_i\\ & - \left[E_{BX}(x_i) + E_{BY}(y_i)\right](t_z + z_i)\\ & + E_{CX}(x_i)\cdot y_i - E_{X0X}\end{aligned} \tag{30}$$

Respectively, i geometric features must be given in the Y-direction at which the X-differences Δx_i can be determined. In order to be able to determine the errors E_{XY} and E_{C0Y} independently of other error factors the X- and Z-positions x_i and z_i of the features must be identical.

As a result, the following simplifications apply:

$$z_i + t_z = z_{m,2} = const. \tag{31}$$

$$x_i = x_{m,2} = const. \tag{32}$$

$$E_{XZ}(z_i) = const. \tag{33}$$

$$E_{B0Z} \cdot z_i = const. \tag{34}$$

$$E_{BX}(x_i) = const. \tag{35}$$

$$E_{CX}(x_i) = const. \tag{36}$$

$$E_{X0X} = const. \tag{37}$$

With these simplifications, Eq. (15) results in

$$\begin{aligned} \Delta x_i = &- E_{XX}(x_{m,2}) - E_{XY}(y_i) \\ &- E_{C0Y} \cdot y_i + E_{BY}(y_i) \cdot z_{m,2} \\ &- E_{CX}(x_{m,2}) \cdot y_i + C_2, \end{aligned} \tag{38}$$

where $x_{m,2}$ and $z_{m,2}$ is the measurement position and C_2 is a constant. As described in Section 3.1.1, the error $E_{XX}(x_i)$ has already been determined on another feature and can be assumed to be known. It is defined that the X-error due to the roll error of the Y-axis $E_{BY}(y_i)$ is zero at the Z-position $Z_{m,2}$, i.e. the error is completely assigned to the straightness error of the Y-axis in the X-direction at this position. Also, it is defined that the X-error due to the yaw error of the X-axis $E_{CX}(x_i)$ is zero at the X-position $X_{m,2}$, i.e. the error is completely attributed to the squareness error of Y to X as well as the straightness error of the Y-axis in the X-direction at this position. With these definitions the equation simplifies to

$$\begin{aligned} \Delta x_i + E_{XX}(x_{m,2}) = &- E_{XY}(y_i) \\ &- E_{C0Y} \cdot y_i + C_2. \end{aligned} \tag{39}$$

From this equation, the straightness error of the Y-axis in the X-direction E_{XY} as well as the squareness error between the Y- and X-axis E_{C0Y} can be determined. To separate the two errors, E_{C0Y} is determined using a linear regression calculation:

$$\| \Delta x_i + E_{XX}(x_{m,2}) + E_{C0Y} \cdot y_i \|_2 \stackrel{!}{=} \min. \tag{40}$$

$EXY(y_i)$ can then be determined by the equation

$$\begin{aligned} \Delta x_i + E_{XX}(x_{m,2}) + E_{C0Y} \cdot y_i = \\ -E_{XY}(y_i) + C_2. \end{aligned} \tag{41}$$

The constant C_2 can be determined by suitable conditions, such as $E_{XY}(y) = 0$ for $y = 0$. These considerations result in the requirement that geometric features in the Y-direction with identical X- and Z-positions must be present at the artifact, whose X-positions can be determined.

The geometric features required to determine the E_{YY} and E_{ZY} errors can be derived in the same way. For these errors, there must be geometric features in the Y-direction with identical X- and Z-positions, whose Y- and Z-positions can be determined. As before, the exact type of geometric features is irrelevant in this context. An example where holes have been used is shown in Fig. 4.

Unlike the X-axis straightness errors, the Y-axis straightness errors are not evaluated relative to the orientation of the coordinate system, but relative to a straight line as the result of a linear regression.

For the derivation of the further geometric features, it can be taken into account that the errors E_{C0Y}, E_{XY}, E_{YY} and E_{ZY} are determined after the measurement of these features and can be assumed as known for further considerations.

3.1.3. Derivation of geometric features for the yaw error of the X-axis

The derivation of the geometric features for determining the yaw error of the X-axis is somewhat different from the previous derivations and is therefore explained below.

The error E_{CX} can be calculated using Eq. (15):

$$\begin{aligned} \Delta x_i = &x_{i,actual} - x_{i,nominal} \\ = &- E_{XX}(x_i) - E_{XY}(y_i) - E_{XZ}(z_i) \\ &- E_{C0Y} \cdot y_i - E_{B0Z} \cdot z_i \\ &- \left[E_{BX}(x_i) + E_{BY}(y_i) \right] \left(t_z + z_i \right) \\ &+ E_{CX}(x_i) \cdot y_i - E_{X0X} \end{aligned} \tag{42}$$

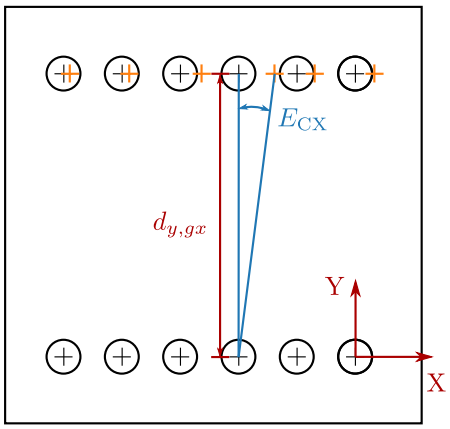

Fig. 5. Example layout of holes in a plate to determine the yaw error of the X-axis.

Consequently, i geometric features must be available in the X-direction at which the X-differences Δx_i can be determined. For the yaw error of the X-axis E_{CX} to be determined independently of other error factors, the Y- and Z-positions y_i and z_i of the features must be identical. In order to measure the influence of the X-yaw error, it is also necessary to measure at a Y-position different from $y_{m,1}$. In total, the simplifications

$$z_i + t_z = z_{m,3} = const. \tag{43}$$

$$y_i = y_{m,3} = y_{m,1} + d_{y,gx} = const. \tag{44}$$

$$E_{XY}(y_i) = const. \tag{45}$$

$$E_{XZ}(z_i) = const., \tag{46}$$

$$E_{C0Y} \cdot y_i = const. \tag{47}$$

$$E_{B0Z} \cdot z_i = const. \tag{48}$$

$$E_{BY}(y_i) = const. \tag{49}$$

$$E_{X0X} = const. \tag{50}$$

apply to this measurement, where $d_{y,gx}$ is the Y-distance of the geometric features to the Y-position of the first feature row in the X-direction $y_{m,1}$. This is illustrated in Fig. 5.

In addition, the error E_{XX} can be assumed to be known as explained above. Thus Eq. (15) results in:

$$\begin{aligned} \Delta x_i + E_{XX}(x_i) + E_{BX}(x_i) \cdot z_{m,3} = \\ E_{CX}(x_i) \cdot (y_{m,1} + d_{y,gx}) + C_3 \end{aligned} \tag{51}$$

For further evaluation it is necessary that the pitch error of the X-axis $E_{BX}(x_i)$ at the Z-position $z_{m,3}$ is zero. It has already been defined in Section 3.1.1 that $E_{BX}(x_i)$ is zero at the Z-position $z_{m,1}$. Therefore, it must apply:

$$z_{m,3} = z_{m,1} \tag{52}$$

In addition, it was defined in Section 3.1.1 that $E_{CX}(x_i)$ is zero at the Y-position $y_{m,1}$. Hence the following applies:

$$E_{CX}(x_i) \cdot y_{m,1} = 0 \tag{53}$$

This results in the following:

$$\Delta x_i + E_{XX}(x_i) = E_{CX}(x_i) \cdot d_{y,gx} + C_3 \tag{54}$$

Accordingly, the error E_{CX} at the positions x_i can be determined by comparing the measured positions $x_{i,actual}$ with the nominal positions $x_{i,nominal}$:

$$E_{CX}(x_i) = \frac{\Delta x_i}{d_{y,gx}} + \frac{E_{XX}(x_i)}{d_{y,gx}} + C_3 \tag{55}$$

The constant C_3 can be specified by appropriate conditions, such as $E_{CX}(x) = 0$ for $x = 0$. Therefore, geometric features in X-direction with identical Y- and Z-positions must be available for the artifact, which have the Y-distance $d_{y,gx}$ from $y_{m,1}$ as well as the same Z-position $z_{m,1}$ and at which the X-position can be determined. As before, the exact type of geometric features is irrelevant in this context.

For the derivation of further geometric features, it can be considered that the error E_{CX} is determined after the measurement of these features and can be assumed as known.

3.1.4. Derivation of geometric features for the pitch and roll error of the X-axis

The derivation of the geometric features to determine the X-axis pitch and roll error differs somewhat from the previous derivations and is therefore explained in the following.

The pitch error of the X-axis E_{BX} can be determined from Eq. (15):

$$\begin{aligned}\Delta x_i =& x_{i,actual} - x_{i,nominal}\\ =& - E_{XX}(x_i) - E_{XY}(y_i) - E_{XZ}(z_i)\\ & - E_{C0Y} \cdot y_i - E_{B0Z} \cdot z_i\\ & - \left[E_{BX}(x_i) + E_{BY}(y_i)\right](t_z + z_i)\\ & + E_{CX}(x_i) \cdot y_i - E_{X0X}\end{aligned} \tag{56}$$

Correspondingly, there must be i geometric features in the X-direction at which the X-differences Δx_i can be determined. In order to determine the pitch error of the X-axis E_{BX} independently of other error factors, the Y- and Z-positions y_i and z_i of the features must be identical. In addition, to be able to measure the X pitch error, the measurement must be made at a Z-position deviating from $z_{m,1}$. Overall, the following simplifications apply:

$$z_i + t_z = z_{m,4} = z_{m,1} + d_{z,nx} = const. \tag{57}$$

$$y_i = y_{m,4} = const. \tag{58}$$

$$E_{XY}(y_i) = const. \tag{59}$$

$$E_{XZ}(z_i) = const., \tag{60}$$

$$E_{C0Y} \cdot y_i = const. \tag{61}$$

$$E_{B0Z} \cdot z_i = const. \tag{62}$$

$$E_{BY}(y_i) = const. \tag{63}$$

$$E_{X0X} = const. \tag{64}$$

Here $d_{z,nx}$ is the Z-distance of the geometric features to the Z-position of the first feature row in X-direction $z_{m,1}$. This is illustrated in Fig. 6. The errors E_{XX} and E_{CX} can be assumed to be known as described above. Furthermore, it was defined in Section 3.1.1 that $E_{BX}(x_i)$ is zero at the Z-position $z_{m,1}$. Hence the following applies:

$$E_{BX}(x_i) \cdot z_{m,1} = 0 \tag{65}$$

This results in

$$\begin{aligned}\Delta x_i + E_{XX}(x_i) - E_{CX}(x_i) \cdot y_{m,4} =\\ -E_{BX}(x_i) \cdot d_{z,nx} + C_4\end{aligned} \tag{66}$$

As before, the X-pitch error E_{BX} at the positions x_i can be determined from this equation by comparing $x_{i,actual}$ and $x_{i,nominal}$ by defining the constant C_4 via a corresponding condition, such as $E_{BX}(x) = 0$ for $x = 0$. As a result, the artifact must have geometric features in the X-direction with identical Y- and Z-positions, which have the Z-distance $d_{z,x}$ from $z_{m,1}$ and at which the X-position can be determined. The exact type of geometric features is irrelevant in this context, as before.

The derivation of the geometric features for the roll error of the X-axis proceeds in an almost identical way. Here, however, the Y-deviations are considered according to Eq. (16). From this it follows that geometric features in the X-direction must be available at the artifact, which have the Z-distance $d_{z,x}$ from the Z-position of the first feature series in the X-direction $z_{m,1}$ and at which the Y-positions can be determined. This is illustrated in Fig. 7.

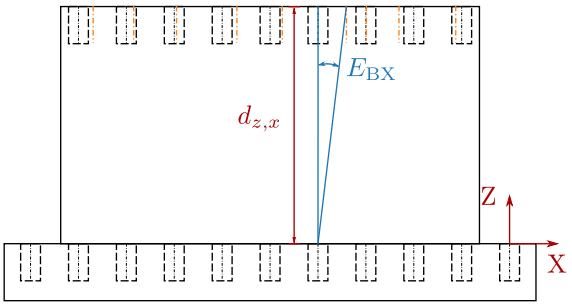

Fig. 6. Example arrangement of holes in two planes to determine the pitch error of the X-axis.

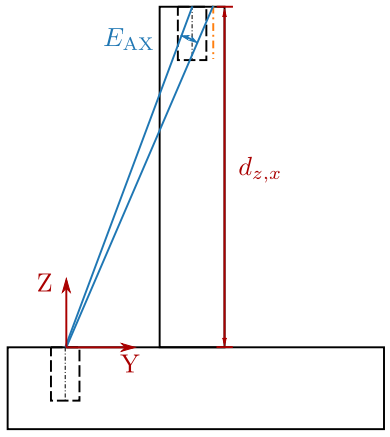

Fig. 7. Example layout of holes in two planes to determine the roll error of the X-axis.

When deriving the further geometric characteristics, it can be assumed as before that the errors E_{BX} and E_{AX} are known after these measurements.

3.1.5. Derivation of further geometric features to determine the remaining errors

The next step is to derive geometric features that can be used to determine the roll error E_{BY} and yaw error E_{AY} of the Y-axis. The derivations are similar to the derivations of the geometric features for the pitch and roll error of the X-axis. Therefore, the derivations are not explained here.

To determine the roll error of the Y-axis E_{BY}, there must be geometric features on the artifact in the Y-direction whose X-positions can be determined, whose Y- and Z-positions are identical and whose Z-distance to the Z-position of the first feature row in the X-direction is $d_{z,x}$. Fig. 8 illustrates this. To be able to determine the yaw error of the Y-axis E_{AY}, there must be geometric features on the artifact in the Y-direction whose Y-positions can be determined, whose Y- and Z-positions are identical and whose Z-distance to the Z-position of the first feature row in the X-direction is equal to $d_{z,y}$. This is shown in Fig. 9.

Once these errors have been determined, the geometric features for determining the positioning and straightness errors of the Z-axis E_{XZ}, E_{YZ}, E_{ZZ} and the squareness errors of the Z-axis to the X- and Y-axis E_{A0Z}, E_{B0Y} can be derived. The derivation of the Z-axis errors is basically identical to the X- and Y-axis. There must be geometric features in the Z direction whose X-, Y- and Z-positions can be determined with a probe. Note, however, that the machine design considered here (see Fig. 3) means that the geometric features must be arranged side by side,

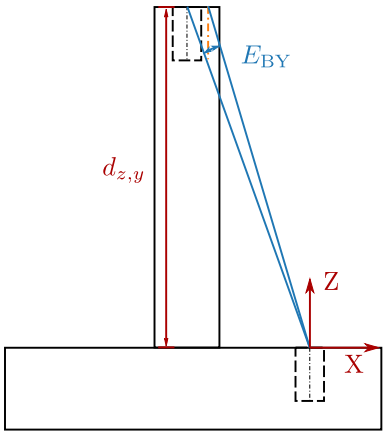

Fig. 8. Example layout of holes in two planes to determine the roll error of the Y-axis.

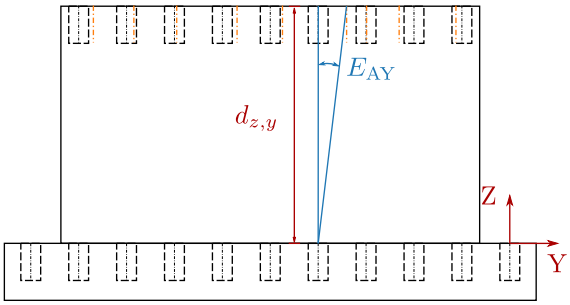

Fig. 9. Example layout of holes in two planes to determine the yaw error of the Y-axis.

e.g. in steps, otherwise they cannot be detected by the 3D touch trigger probe. These geometric features can be arranged in either the X or Y direction.

Moving two axes (X- and Z-axis or Y- and Z-axis) is not a problem at this stage as the errors of the X- and Y-axis are already known. An example of a possible arrangement of the geometric features is shown in Fig. 10. Here, a step triangle in the X-direction is used, in which bore holes are provided whose position can be detected with the probe.

Finally, the zero displacement E_{X0X}, E_{Y0Y} and E_{Z0Z} described in Section 2.2 can be determined on any geometric feature whose X-, Y- and Z-position can be measured.

3.1.6. Design of the entire artifact

In the previous sections, geometric features were derived to determine all relevant geometric machine errors. These geometric features are combined into one artifact at this point. For this purpose, VDI/VDE 2617 part 5 [40], which describes the intermediate testing of CMMs on the basis of artifacts, is taken into account. This document describes the requirements for the artifacts, e.g. that the artifacts must be stable, the coefficient of thermal expansion must be known and the features to be inspected must be designed in such a way that the specified accuracy in determining their positions can be achieved. These requirements can be met by the choice of material, fixtures, features and the machining quality.

For the artifact presented in this paper, Invar was chosen as the material for the artifact. This material combines a low coefficient of thermal expansion (CTE) of $0.8\,\mu m/(m\,K)$ for temperatures between $20\,°C$ and $50\,°C$ [45] with good machinability. Bore holes and planes are used as features to be probed. Their positions are clearly definable. A bore hole and a plane each represent a point in space.

The artifact is designed as follows: A square plate is chosen as the basic body. Two further plates and a step triangle are attached to it in such a way that they meet at one edge each. In the base plate as well as in the mounted plates and the step triangle there are bore holes whose X- and Y-positions can be determined with a measuring probe. Next to each bore hole is an area of high surface quality where the Z-position can be measured. Fig. 10 shows a 3D CAD model of the artifact. The openings in the base plate shown in the 3D CAD model are only there to save weight.

The artifact presented here has a modular design and can be adapted to the size of the work area of the MT. In this way, the artifact can be scaled for the particular machine to be examined. This provides great flexibility in terms of the MTs that can be studied with the artifact. The number and size of the bore holes are also flexible and should be chosen according to the size of the artifact and the accuracy requirements.

4. Identification of geometric errors

This section explains how the geometric errors of a MT can be identified with the artifact presented in Section 3.1.6. The artifact is first measured once on a CMM to determine the nominal positions of the geometric features. This measurement therefore represents the calibration of the artifact. The advantage of this procedure is that it simplifies the production of the artifact, as the positional tolerances of the geometric features can be much greater in comparison to when the artifact is not previously calibrated. Subsequently, the artifact can be set up and measured on any 3-axis portal milling machine in table design. These measurements are used to record the actual positions of the geometric features on the respective MT. By comparing the nominal and actual positions, the relevant geometric errors can be determined using the formulas derived in Section 3. The determined errors can then be mathematically processed and transmitted to the CNC control as correction values. A significant advantage of the measurement method is that the measurement of the actual positions of the features can be repeated cyclically. This allows the geometric errors and their changes to be observed over a long period of time. This makes it possible to investigate thermoelastic defects.

The complete identification process is shown as a flowchart in Fig. 11.

4.1. Measurement process

The measurement of the geometric features of the artifact is performed identically when calibrating the artifact on the CMM and when measuring on the MT. The measurement process is described in the following for a machine with three linear axes (X, Y, Z), where the X- and Y-axes move horizontally and the Z-axis moves vertically. This corresponds to the kinematics for which the error model was derived (compare Section 2.2). A 3D touch trigger probe, which is available in most CMMs and MTs, is used to measure the positions of the geometric features. The X- and Y-positions of the geometric features are the centers of the bore holes. These centers are determined with two probing points per axis direction. The Z-positions of the geometric features are surfaces next to the bore holes. The Z-positions of these surfaces are determined with one touch point per feature. The measuring process is composed of the following steps:

1. First, the artifact is set up on the machine. The axes of the local coordinate system of the artifact (see Fig. 10) are aligned parallel to the axes of the machine coordinate system according to common workshop practice. Due to the adjustment of the coordinate system in the next step, the accuracy of the presented method is not affected by a non-ideal alignment.
2. In the next step, the artifact coordinate system must be adjusted to the orientation of the artifact in order to correct inaccuracies of the orientation of the artifact. For this purpose, the Z-positions of features 1, 18, 35 and 52 are determined in the corners of the base plate. A correction plane is placed through these Z-positions, on which the artifact coordinate system is aligned so

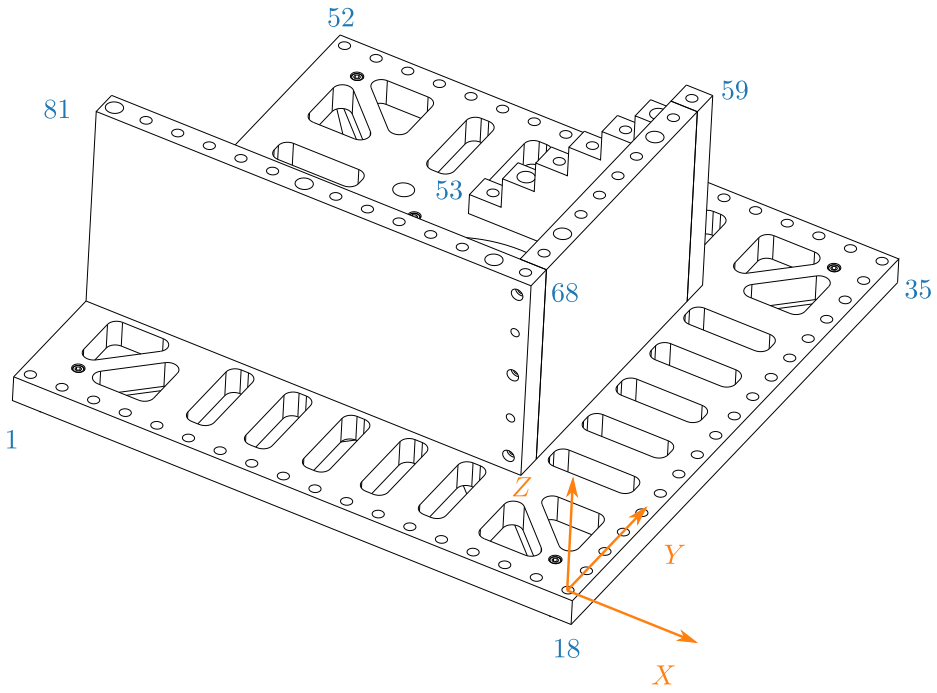

Fig. 10. 3D CAD model of the artifact with local coordinate system and feature numbering.

that the XY-plane of the coordinate system is parallel to the base plate of the artifact. Then the X- and Y-positions of the geometric features 1 and 18 in the base plate are measured. With these results, the artifact coordinate system is rotated in the XY-plane so that the X-axis of the coordinate system passes through these two features. In the last step, the X-, Y- and Z-position of feature 1 in the base plate are measured and the zero point of the artifact coordinate system is moved to this position. In this way, the coordinate system used for the error evaluation described in Section 3.1 is determined.

3. After that, the actual measurement of the positions of the geometric features is performed. The machine automatically moves to all feature positions one after the other by using a suitable NC program and measures their positions. The determined feature positions are stored digitally and processed further, depending on whether it is a calibration process or an error detection.

If the geometric errors should be measured over a long period of time, as is necessary, for example, for the investigation of thermal machine behavior, step 3 of the measurement process must be repeated cyclically. In addition, if the thermal behavior of the machine is to be investigated, it is usually necessary to record additional data such as temperatures.

4.2. Identification of the geometric errors

In order to identify the geometric errors of a MT, the measurement process described in Section 4.1 must have been carried out at least once on a CMM and once on the MT to be examined. The measurement of the artifact on a CMM is used as a reference measurement. This provides the nominal positions of the geometric features. The measurement of the artifact on the MT gives the actual positions of the geometric features. With this data, the differences between actual and nominal positions

$$\begin{aligned} \Delta x_i &= x_{i,actual} - x_{i,nominal} \\ \Delta y_i &= y_{i,actual} - y_{i,nominal} \\ \Delta z_i &= z_{i,actual} - z_{i,nominal} \end{aligned} \tag{67}$$

can be calculated for all i features. Based on these differences, the geometric errors of the examined MT can be calculated using the equations derived in Section 3.1. For example, 18 pairs of values $(x_i, EXX(x_i))$ with $i = 1, \ldots, 18$ result for the X positioning error. Between these discrete points, interpolation can be performed, for example, using spline interpolation.

4.3. Consideration of thermal artifact expansion

The artifact expands depending on its temperature. Although a material with a low coefficient of thermal expansion is used, this expansion must be taken into account, especially in thermal investigations.

Modern CMMs typically have a built-in system to correct the thermal expansion of the object to be measured. Here, the artifact temperature is measured and the output positions of the features are automatically adjusted to the reference temperature of 20 °C using the thermal expansion coefficient.

In contrast to CMMs, MTs do usually not have such a correction system [46]. Therefore, the measured feature positions must be adjusted based on the artifact temperature before further processing. The material of the artifact is Invar 36 with a CTE of $\alpha \approx 1.6\,\mu m/(m\,K)$ (see Section 3.1.6). To correct this, the measured feature positions must be shifted according to their distance d to the zero point of the artifact coordinate system on the connecting line between feature and zero point so that a linear approximation

$$d_{corr} \approx d \cdot \left[1 - \alpha \left(\vartheta_{wp} - \vartheta_{ref}\right)\right] \tag{68}$$

is the new distance to the zero point, where ϑ_{wp} is the artifact temperature, which is taken from simultaneous measurement. In this way, the positions of the features are corrected to the reference temperature of $\vartheta_{ref} = 20\,°C$ for further calculation.

Both the CMMS temperature correction and the correction described here are only valid for constant temperatures. They are not fully valid for temperature changes and are not valid if the temperature changes are within the time constants of the components involved.

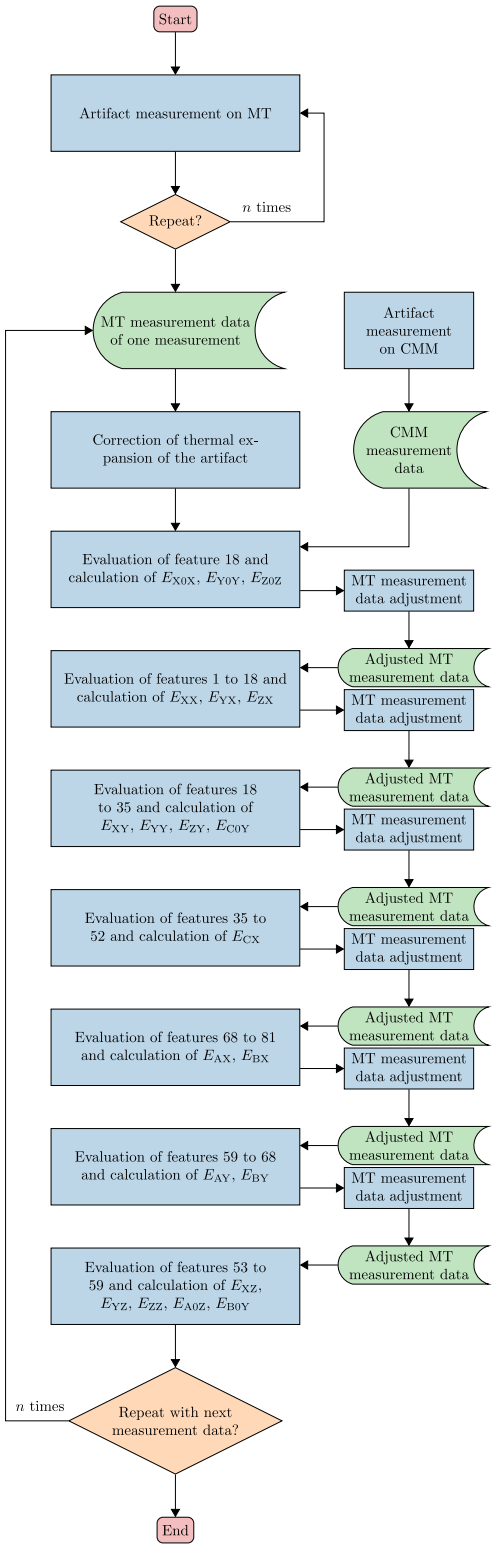

Fig. 11. Geometric error identification flowchart.

5. Experimental investigation of thermo-elastic machine behavior

Artifact measurement has already been shown to be generally suitable for measuring geometric machine errors [13,23,47,48]. Therefore, in this section, the suitability of the artifact for the investigation of thermo-elastic machine behavior is examined. For this purpose, a MT in a temperature chamber is exposed to a ambient thermal load and its geometric errors are measured with the artifact presented in Section 3.1.6.

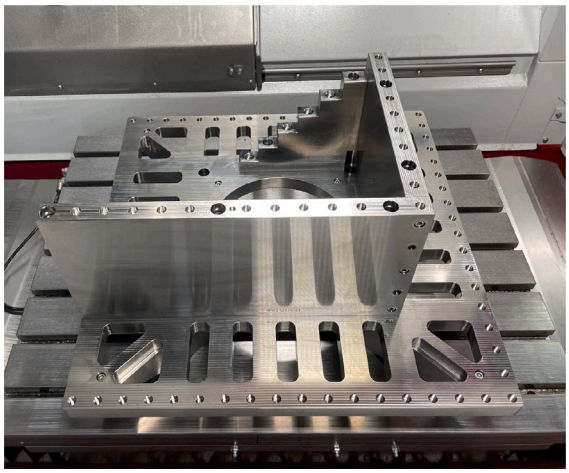

Fig. 12. Artifact.

5.1. Measurement setup and implementation

For the investigations presented below, an artifact was produced consisting of a square base plate with a side length of 530 mm. The other plates and the step triangle, which are mounted on the base plate, have a height of 200 mm. All parts are made of Invar. A total of 81 bore holes have been worked into the artifact (compare Fig. 10). The bore holes have a diameter of 10 mm. Five bore holes have a diameter of 15 mm, because these holes are additionally used for screws to connect the individual parts of the artifact. The surface of the holes and the surfaces adjacent to the holes in the plates are milled. In this way, a high surface quality of $R_a < 0.08\,\mu m$[1] was achieved for all surfaces. The produced artifact is shown in Fig. 12 on the machine table of the MT under test.

The test machine is a 3-axis portal milling machine in table design. The working area of the machine is 800 mm × 635 mm × 400 mm. The dimensions of the machine table are 796 mm × 596 mm and can load workpieces up to 800 kg. The machine operates in a feed range from 0 to 60 000 mm/min and is equipped with an HSK50 milling spindle with a power of 15 kW and a maximum speed of 36 000 1/min. The machine bed and portal are made of polymer concrete, which gives the machine a weight of approximately 8.4 t. The machine is equipped with a Renishaw OMP400 3D touch trigger probe. In addition, the machine is equipped with a temperature measurement system. This consists of two Pt1000 temperature sensors. One sensor measures the ambient air temperature at the front of the machine. The second sensor measures the temperature of the workpiece and can be magnetically attached to the workpiece.

The test machine is examined in a temperature chamber. Inside this chamber, the ambient temperature can be set to any level between 20 °C and 30 °C, while the airflow remains constant. This allows the thermo-elastic machine behavior to be investigated under ambient temperature changes.

To perform the measurement, the artifact is fixed to the machine table with four screws, which are placed in the center of the artifact at a small distance from each other. In this way, it is assumed that the machine table and the artifact are largely independent of each

[1] Measured with ZEISS Surfcom 2000SD.

other in terms of deformation. A more detailed consideration of the deformation of the artifact due to different coefficients of expansion of the machine table and the artifact was not carried out within the scope of this paper. The temperature in the temperature chamber is first set to a constant temperature of 23 °C. Then, 36 h are waited until the machine has reached a thermally stable state. The measuring process is then started as described in Section 4.1 and step 3 of the measurement process is repeated cyclically. For the first 12 h, the temperature of the temperature chamber is still set to 23 °C. Then a sinusoidal temperature profile with an amplitude of 3 K and a period of 24 h is operated for a total of 120 h. This corresponds to a typical day-night temperature pattern. Subsequently, the temperature is set to 23 °C for 12 h. During the entire measurement, the temperatures are recorded with the integrated measuring system.

5.2. Measurement uncertainty

As described in Section 4.2, the geometric errors result directly from the measured positions of the features of the artifact. These positions are subject to measurement uncertainty. The measurement uncertainty consists of uncontrollable random measurement errors as well as known and unknown systematic measurement errors. The evaluation of the measurement uncertainty is carried out according to ISO/IEC Guide 98-3:2008 (GUM) [49].

5.2.1. Systematic measurement errors

The systematic measurement error is a component of the measurement error that in replicate measurements remains constant or varies in a predictable manner [50]. If a systematic error arises from a recognized effect of an influence quantity on a measurement result, the effect can be quantified and a correction can be applied to compensate for the effect. Systematic errors themselves are subject to uncertainty [49].

As described in Section 4.3, the measured feature positions must be corrected for thermal artifact expansion before further processing. The CTE is generally subject to an uncertainty due to the exact composition and manufacture of Invar 36. According to the supplier, the Invar conforms to SEW 385:1991. This standard specifies a permissible range of $\Delta\alpha = \pm 0.3\,\mu m/(m\,K)$ as uncertainty for the CTE [45]. From this, a standard uncertainty of $u(\alpha) = 0.17\,\mu m/(m\,K)$ is estimated according to ISO/IEC Guide 98-3:2008 Type B evaluation of standard uncertainty [49].

In addition, the temperature measurement system of the MT may contain a systematic error. The manufacturer specifies a range of $\Delta\vartheta = \pm 0.3$ K as uncertainty for the temperature measurement system. According to ISO/IEC Guide 98-3:2008 this gives a standard uncertainty of $u(\vartheta_{wp}) = 0.17$ K [49]. Applying ISO/IEC Guide 98-3:2008 to Eq. (68) gives the combined standard uncertainty of

$$u_c^2(d_{corr}) = c_\alpha^2 u^2(\alpha) + c_{\vartheta_{wp}}^2 u^2(\vartheta_{wp}), \tag{69}$$

with

$$c_\alpha = \frac{\partial d_{corr}}{\partial \alpha} = d \cdot \Delta\vartheta, \tag{70}$$

$$c_{\vartheta_{wp}} = \frac{\partial d_{corr}}{\partial \vartheta_{wp}} = d \cdot \alpha. \tag{71}$$

So $u_c^2(d_{corr})$ depends on the distance d, the temperature difference $\Delta\vartheta$ and the CTE α. As described in Section 5.3, the change in machine geometry under the influence of ambient temperature changes is investigated. Therefore, the measured temperature difference of the artifact during the measurement can be used for $\Delta\vartheta$. $u_c^2(d_{corr})$ must be calculated individually for each feature measurement. With a maximum distance d of 720 mm and a maximum temperature difference $\Delta\vartheta$ of 1.5 K, an upper limit value of $u_c(d_{corr}) \leq 0.2\,\mu m$ can be estimated.

However, as described in Section 5.3, the machine geometry is not compared with a reference measurement, but with the change in machine geometry under the influence of ambient temperature changes (see Eq. (76)). Therefore, on the one hand, the measurement uncertainty of the reference measurement can be neglected in this investigation and, on the other hand, it can be assumed that no further systematic effects influence the measurement. The influence of random errors will be discussed in the next section. However, as the uncertainty of an unknown systematic effect, an additional standard uncertainty u_{sme} is included. For Renishaw's OMP400 touch-trigger 3D probe, the manufacturer claims a repeatability of $\pm 0.25\,\mu m$, which corresponds to a standard uncertainty of $u_{probe} = 0.14\,\mu m$ according to ISO/IEC Guide 98-3:2008 [49,51]. This value gives an indication. The u_{sme} is therefore estimated to be $0.2\,\mu m$.

5.2.2. Random measurement errors

In order to estimate the random measurement errors, the measurements at constant ambient temperature are evaluated. The MT is assumed to be thermally stable at constant temperature after the 36-hour waiting period. Therefore, the measured values from the period between $t = 0$ h and $t = 12$ h are used to calculate the standard uncertainty. The series of measurements yields 454 measured values for the positions $x_{i,j}$, $y_{i,j}$, $z_{i,j}$ of each feature i. It is assumed that the measurement values are normally distributed.

According to ISO/IEC Guide 98-3:2008 Type A evaluation of standard uncertainty [49], the experimental standard deviation of the distribution of measured values for each feature i can be calculated using

$$s_{0,i} = \sqrt{\frac{1}{n-1}\sum_{j=1}^{n}(p_{i,j} - \bar{p})^2} \tag{72}$$

with $p \in (x, y, z)$ and $n = 389$. The experimental standard deviation includes the random errors of all components involved in the measuring process, such as MT and 3D touch trigger probe.

The standard uncertainty can be calculated according to ISO/IEC Guide 98-3:2008 Type A evaluation of standard uncertainty [49] with equation

$$u_{p,i} = \frac{s_{0,i}}{\sqrt{n_i}} \tag{73}$$

for each feature, where n_i is the number of measurements, if the experimental standard deviations of the distributions of the measured values of the input variables are known. For the investigation of the thermoelastic machine behavior, only one measurement at a time is evaluated in order to avoid transient thermal influences on the measurement result. Accordingly, $n_i = 1$ and $u_{p,i} = s_{0,i}$ follow.

The values for $u_{p,i}$ are different for each feature i and axis $p \in (x, y, z)$. The values are between 0.10 µm and 0.25 µm.

5.2.3. Measurement uncertainty

According to ISO/TR 230-9:2005 [52], the measurement uncertainty U_i of the feature positions i is determined by the following equation:

$$U_i = k \cdot u_{c,i} \tag{74}$$

The coverage factor k is set to 2 and u_c is the combined standard uncertainty of the feature positions. The combined standard uncertainty of the feature positions $u_{c,i}$ is calculated according to ISO/IEC Guide 98-3:2008 as the squared combination of the individual uncertainties:

$$u_{c,i} = \sqrt{u_c^2(d_{corr}) + u_{sme}^2 + u_{p,i}^2}, \tag{75}$$

Fig. 13 shows the measurement uncertainties U for all feature positions, calculated with a maximum temperature difference $\Delta\vartheta$ of 1.5 K and assuming 0.2 µm for u_{sme}. The values for $u_c(d_{corr})$ and $u_{p,i}$ are calculated as described above. An upper limit of $U \leq 0.75\,\mu m$ with $k = 2$ can be estimated.

The measurement uncertainty is related to the distance d between the feature and the zero point. It increases with increasing distance d. The reason for this is the standard uncertainty $u_c(d_{corr})$, which depends on the distance d.

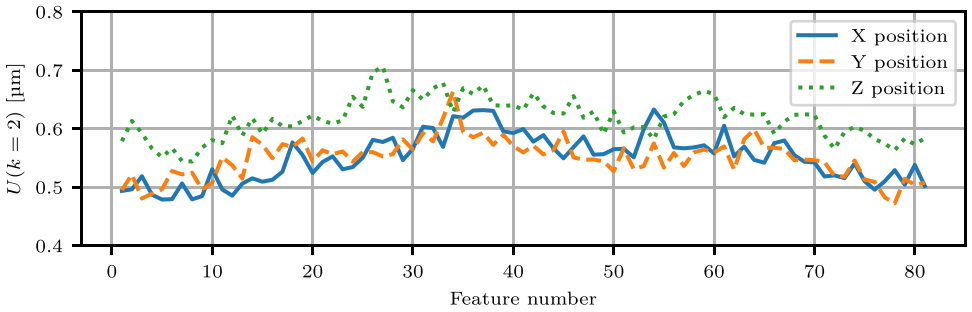

Fig. 13. Measurement uncertainty U with $k = 2$. Used calculated values for $u_c(d_{corr})$ with a maximum temperature difference $\Delta\vartheta$ of 1.5 K, assumption of 0.2 µm for u_{sme} and calculated values for $u_{p,i}$.

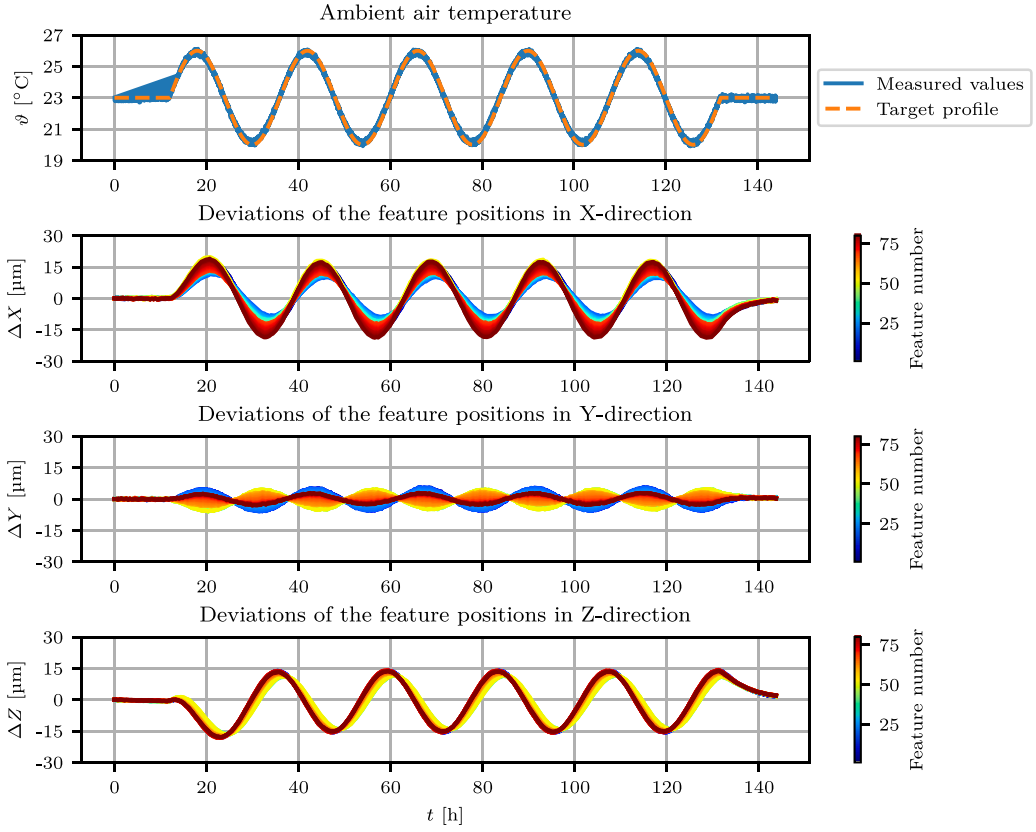

Fig. 14. Air temperature and measured deviations of the axes sorted by position of the features.

5.3. Measurement results

Fig. 14 shows the measured values of the investigation. The top subplot shows the air temperature measured by the temperature sensor of the MT. It can be seen that the measured temperatures follow the target profile of the climate chamber. The lower three subplots show the measured deviations of the feature positions in the X-, Y- and Z-directions. The deviations are the change in the respective feature position compared to time $t = 0$. Thus, the following applies:

$$\Delta p_i(t) = p_i(t) - p_i(0) \tag{76}$$

where $p \in (x, y, z)$ and i is the number of the respective feature. The machine geometry is therefore not compared with a reference measurement, but the change in machine geometry under the influence of ambient temperature changes is considered. The colors of the curves indicate the number of the respective feature (compare Fig. 10). The more the graphs of the individual features deviate, the more the corresponding deviation is position-dependent. The deviations show a delay in time in relation to the air temperature. This is probably due to the inertia of the polymer concrete machine components (see Section 5.1). A precise analysis of the thermal behavior of the MT is beyond the scope of this paper.

Based on these data, all relevant geometric errors are calculated for each time point according to Section 4. Thereby, the constant C_i in the respective equations is chosen such that the respective geometric error at the origin is zero (compare Section 4). Fig. 15 shows all relevant component errors as an example at time $t = 24$ h. The location errors are not shown in the figure as they are single values. These errors are plotted over time in Fig. 16. The error bars indicate the measurement uncertainty (compare Section 5.2). Cubic splines were used to interpolate between the individual measurement points.

With the presented method, all relevant geometry errors are known at any time. Due to the change in thermal load, the individual error changes continuously, which can be measured using the method. The errors with the greatest influence on the machine geometry during the performed measurement are plotted in Fig. 16 as an example.

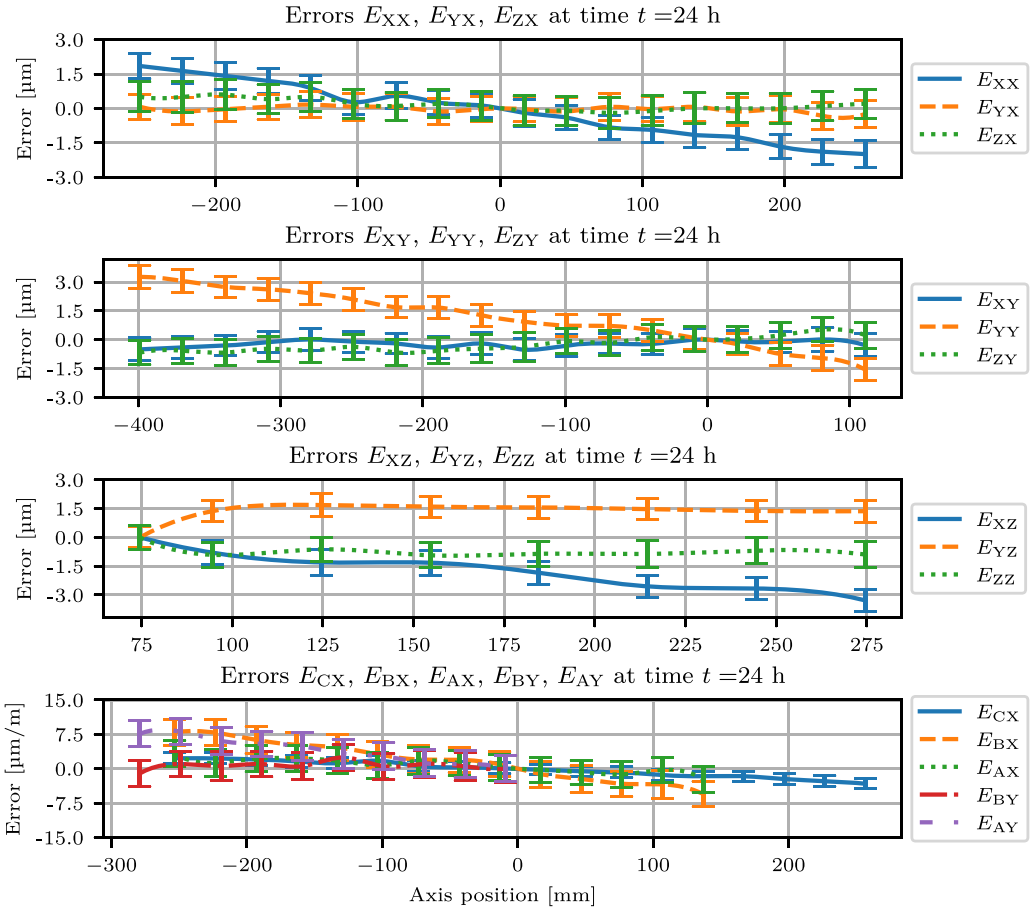

Fig. 15. Errors and combined standard uncertainties u_c as bars at time $t = 24$ h. Used assumption of 0.2 µm for u_{sme} and calculated values for $u_c(d_{corr})$ and $u_{p,i}$.

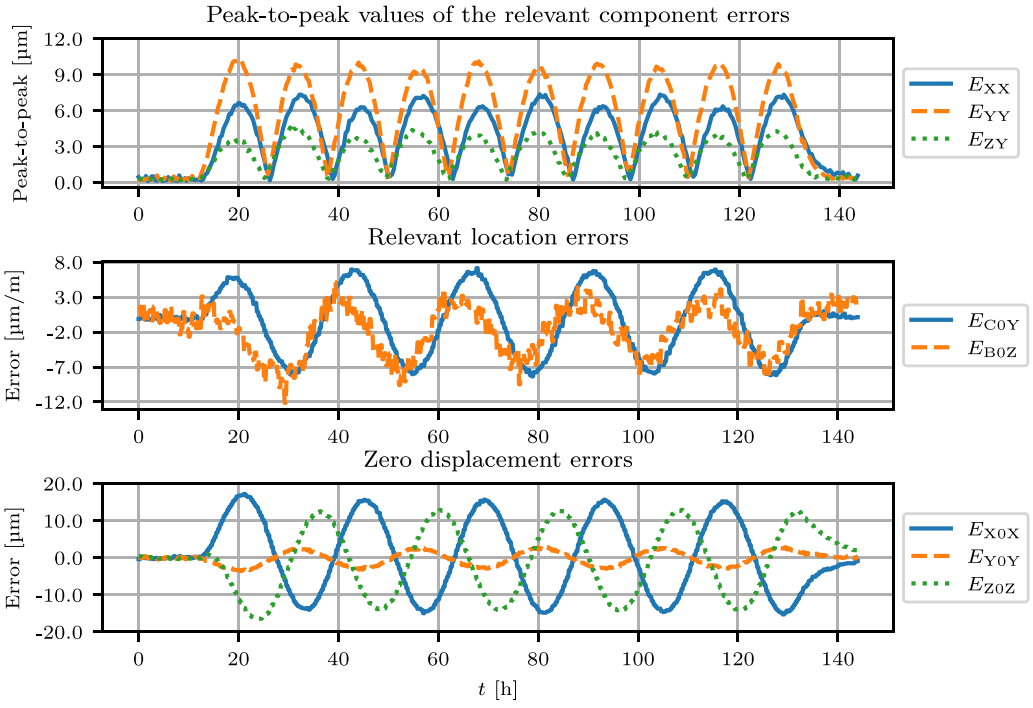

Fig. 16. Relevant errors over time.

As described before, the component errors are position dependent. Therefore, the relevant component errors are shown in the top subplot as peak-to-peak values of the corresponding features evaluated, which represents the error span at each time point.

In addition to the measurement results, the duration of a single measurement was recorded. It is about 12 min for this measurement setup and machine configuration.

6. Discussion

Breitzke and Hintze presented a comparable artifact-based measurement method in [23] and compared it with conventional measuring devices according to ISO 230-1:2012 [15]. The measurement method presented in [23] requires that the roll and tilt errors of all axes have already been measured and are negligibly small. As a result, the method has limited applicability for long-term measurements such as those required to study thermo-elastic machine behavior, since the influence of roll and tilt errors is not known. With the artifact presented in this paper it is possible to measure all relevant errors. However, the comparability with conventional measurement devices remains, as do the advantages and disadvantages explained in [23]. Therefore, this discussion will focus on the suitability of the presented artifact-based measurement method for the investigation of thermo-elastic machine behavior.

Using the artifact, it is possible to evaluate the thermo-elastic machine behavior with respect to ambient temperature effects, as can be seen in Section 5. For this purpose, the geometric machine errors of a MT are measured cyclically.

An important aspect of whether measurement methods are suitable for measuring thermo-elastic errors is a sufficiently short measurement time so that transient thermo-elastic displacements during the measurement only influence the measurement result to a negligible degree [6]. The determined duration of 12 min for a single measurement can be considered sufficiently short for thermo-elastic errors to be identified in the investigated measurement setup. To determine this, a step response was recorded in the climate chamber in a second experiment, which will not be discussed in detail in this paper. Based on the measurement results, the geometric errors were modeled using PT1 elements. The duration of a single measurement is only about 10 % of the smallest time constant of the PT1 elements and can therefore be considered sufficiently short. This can be further optimized by, for example, adjusting the feed rates or the pre-positioning of the probe. Accordingly, the change in geometric errors within a single measurement can be considered sufficiently small.

The determined measurement uncertainties (compare Fig. 13) can also be considered sufficiently small for the identification of the geometric errors.

At this point it should be noted that both the measurement duration and the measurement uncertainty depend on the specific artifact size and number of bore holes, on the MT and the probe. Accordingly, both properties must be re-evaluated for each measurement setup.

If the properties (measurement duration, measurement uncertainty) are given, the presented method offers a cost-effective, multi-purpose method for the measurement of thermo-elastic errors. In comparison with existing artifact-based measurement methods for measuring thermo-elastic errors (compare [18–22]), the major advantage of the presented method is that all relevant geometric errors are covered. Thus, a more comprehensive understanding of the thermo-elastic machine behavior can be obtained.

The disadvantage of all artifact-based measurement methods, including the method presented in this paper, is that the investigation of internal heat sources is limited because it is not possible to measure feature positions and axis movement or motor spindle operation at the same time. To investigate the influence of internal heat sources, intermediate measurements must be made. For example, to investigate the influence of the motor spindle, the spindle must be switched on, run at a defined speed for a defined time, switched off and then a measurement can be performed. Intermediate measurements are allowed according to ISO 230-3:2020 [10]. However, this is a limitation.

Therefore, potential applications are primarily the investigation of the thermal behavior of the machine under workshop conditions and the regular calibration of the machine geometry to ensure the accuracy of the machine.

7. Conclusion

In this paper, based on the modeling of geometric errors, a new design for a three-dimensional artifact for measuring geometric errors was derived. This makes it possible to identify all relevant geometric errors of three-axis portal milling machines in table design. The presented measurement method is thus suitable for both the one-time identification of geometric errors and for the investigation of thermo-elastic machine behavior, in which the measurement is repeated cyclically. In particular, this paper addressed the aspect of the method's suitability for thermo-elastic investigations. For this purpose, the derived artifact was produced and measured in a MT in a temperature chamber with changing thermal load. In this way, the behavior of the MT at changing ambient temperature was investigated. The measurement results were presented and the suitability of the measurement method for the investigation of thermo-elastic machine behavior was discussed. It can be concluded that the measurement method is particularly suitable for the investigation of thermo-elastic machine behavior due to the following properties:

- The measurement duration is sufficiently short (approximately 12 min) so that transient thermo-elastic displacements influence the measurement result to a negligible degree.
- The measurement uncertainty is sufficiently low ($U \leq 0.75\,\mu m$ with $k = 2$) so that a reliable identification of the geometric errors is possible.
- All relevant geometric errors for the investigated machine type can be measured, so that a comprehensive understanding of the thermo-elastic machine behavior is possible.
- The artifact size can be adapted to the machine size, so that the process can be implemented well for different machines.
- The costs for the production of the artifact and for the required measuring equipment are relatively low.

In summary, this paper was able to derive an artifact-based measurement method for measuring thermo-elastic errors, which enables the investigation of thermal machine behavior on small and medium-sized MTs with low effort and costs.

It is planned to use the developed artifact to investigate the thermal machine behavior in case of ambient temperature changes for different machines, mainly differing in size. For this purpose, artifacts of different sizes will be produced. The measured data from these investigations can then be used as a basis for the development of a control-integrated correction.

Declaration of competing interest

Andre Breitzke reports equipment, drugs, or supplies was provided by Röders GmbH. Andre Breitzke reports a relationship with Röders GmbH that includes: employment.

Appendix. Derivation of kinematic error model

A.1. Ideal coordinate transformations

The matrix describing the transformation from the workpiece coordinate system to the reference coordinate system is:

$$\boldsymbol{T}^{r}_{w} = \begin{bmatrix} 1 & 0 & 0 & w_x \\ 0 & 1 & 0 & w_y \\ 0 & 0 & 1 & w_z \\ 0 & 0 & 0 & 1 \end{bmatrix}, \tag{A.1}$$

where w_x, w_y, w_z is the offset of the workpiece coordinate system with respect to the reference coordinate system, described in the reference coordinate system.

The matrices describing the ideal transformations between the coordinate systems are:

$$\boldsymbol{T}^{r}_{x,ideal} = \begin{bmatrix} 1 & 0 & 0 & x \\ 0 & 1 & 0 & 0 \\ 0 & 0 & 1 & 0 \\ 0 & 0 & 0 & 1 \end{bmatrix} \tag{A.2}$$

$$\boldsymbol{T}^{x}_{y,ideal} = \begin{bmatrix} 1 & 0 & 0 & 0 \\ 0 & 1 & 0 & y \\ 0 & 0 & 1 & 0 \\ 0 & 0 & 0 & 1 \end{bmatrix} \tag{A.3}$$

$$\boldsymbol{T}^{y}_{z,ideal} = \begin{bmatrix} 1 & 0 & 0 & 0 \\ 0 & 1 & 0 & 0 \\ 0 & 0 & 1 & z \\ 0 & 0 & 0 & 1 \end{bmatrix} \tag{A.4}$$

The transformation matrix from the tool coordinate system to the Z-axis coordinate system is given by:

$$\boldsymbol{T}^{z}_{t} = \begin{bmatrix} 1 & 0 & 0 & 0 \\ 0 & 1 & 0 & 0 \\ 0 & 0 & 1 & t_z \\ 0 & 0 & 0 & 1 \end{bmatrix}, \tag{A.5}$$

where t_z is the offset in Z-direction of the tool coordinate system with respect to the Z-axis coordinate system, described in the Z-axis coordinate system.

The ideal transformation matrix $\boldsymbol{T}^{t}_{w,ideal}$, which transforms from the workpiece to the tool coordinate system, results as follows:

$$\begin{aligned} \boldsymbol{T}^{t}_{w,ideal} =& \boldsymbol{T}^{t}_{z}\, \boldsymbol{T}^{z}_{y,ideal}\, \boldsymbol{T}^{y}_{x,ideal}\, \boldsymbol{T}^{x}_{r,ideal}\, \boldsymbol{T}^{r}_{w} \\ =& (\boldsymbol{T}^{z}_{t})^{-1}\, (\boldsymbol{T}^{y}_{z,ideal})^{-1}\, (\boldsymbol{T}^{x}_{y,ideal})^{-1} \\ & (\boldsymbol{T}^{r}_{x,ideal})^{-1}\, \boldsymbol{T}^{r}_{w} \\ =& \begin{bmatrix} 1 & 0 & 0 & w_x - x \\ 0 & 1 & 0 & w_y - y \\ 0 & 0 & 1 & -t_z + w_z - z \\ 0 & 0 & 0 & 1 \end{bmatrix} \end{aligned} \tag{A.6}$$

A.2. Real coordinate transformations

The transformation matrix from the workpiece coordinate system to the reference coordinate system and the transformation matrix from the tool coordinate system to the Z-axis coordinate system are identical for the real and the ideal machine. Cardan angles are used to derive the real transformations. The cardan angles are a set of three angles with which the orientation (rotational position) of a solid body in three-dimensional Euclidean space can be described. All three rotations are rotated around different coordinate axes. According to the z-y'-x'' convention (roll, pitch and yaw angles), the coordinate transformation from the body-fixed to the space-fixed coordinate system is given by the matrix

$$\boldsymbol{R}_{GNR} = \begin{bmatrix} 1 & -E_{\mathrm{Cj}} & E_{\mathrm{Bj}} \\ E_{\mathrm{Cj}} & 1 & -E_{\mathrm{Aj}} \\ -E_{\mathrm{Bj}} & E_{\mathrm{Aj}} & 1 \end{bmatrix}, \tag{A.7}$$

with $j \in (X, Y, Z)$, if small angles are assumed and the simplification

$$\begin{aligned} &\cos(E_{\mathrm{ij}}) \approx 1, \\ &\sin(E_{\mathrm{ij}}) \approx E_{\mathrm{ij}}, \\ &\quad E^{n}_{\mathrm{ij}} \approx 0 \quad \text{für} \quad n > 2, \end{aligned} \tag{A.8}$$

with $i \in (A, B, C)$ and $j \in (X, Y, Z)$ is valid.

For the real transformation matrix that transforms the X-axis coordinate system into the reference coordinate system, the following applies:

$$\boldsymbol{T}^{r}_{x,real} = \begin{bmatrix} \boldsymbol{R}^{r}_{x}(x) & \boldsymbol{r}^{r}_{x} \\ \boldsymbol{0} & 1 \end{bmatrix} \tag{A.9}$$

The matrix $\boldsymbol{R}^{r}_{x}(x)$ results from the matrix $\boldsymbol{R}_{GNR}(x)$ which transforms from the body-fixed X-axis coordinate system to the space-fixed reference coordinate system:

$$\boldsymbol{R}^{r}_{x}(x) = \boldsymbol{R}_{GNR}(x) = \begin{bmatrix} 1 & -E_{\mathrm{CX}}(x) & E_{\mathrm{BX}}(x) \\ E_{\mathrm{CX}}(x) & 1 & -E_{\mathrm{AX}}(x) \\ -E_{\mathrm{BX}}(x) & E_{\mathrm{AX}}(x) & 1 \end{bmatrix} \tag{A.10}$$

In addition:

$$\boldsymbol{r}^{r}_{x} = \begin{bmatrix} E_{\mathrm{XX}}(x) + E_{\mathrm{X0X}} + x \\ E_{\mathrm{YX}}(x) \\ E_{\mathrm{ZX}}(x) \\ 1 \end{bmatrix} \tag{A.11}$$

This results in $\boldsymbol{T}^{r}_{x,real}$ becoming:

$$\boldsymbol{T}^{r}_{x,real} = \begin{bmatrix} \boldsymbol{R}^{r}_{x}(x) & \boldsymbol{r}^{r}_{x} \\ \boldsymbol{0} & 1 \end{bmatrix} = \begin{bmatrix} 1 & -E_{\mathrm{CX}}(x) & E_{\mathrm{BX}}(x) & \beta \\ E_{\mathrm{CX}}(x) & 1 & -E_{\mathrm{AX}}(x) & E_{\mathrm{YX}}(x) \\ -E_{\mathrm{BX}}(x) & E_{\mathrm{AX}}(x) & 1 & E_{\mathrm{ZX}}(x) \\ 0 & 0 & 0 & 1 \end{bmatrix} \tag{A.12}$$

with

$$\beta := E_{\mathrm{XX}}(x) + E_{\mathrm{X0X}} + x. \tag{A.13}$$

In the same way, the other real transformation matrices result in:

$$\boldsymbol{T}^{x}_{y,real} = \begin{bmatrix} \boldsymbol{R}^{x}_{y}(y) & \boldsymbol{r}^{x}_{y} \\ \boldsymbol{0} & 1 \end{bmatrix} = \begin{bmatrix} 1 & -E_{\mathrm{CY}}(y) & E_{\mathrm{BY}}(y) & \chi \\ E_{\mathrm{CY}}(y) & 1 & -E_{\mathrm{AY}}(y) & \delta \\ -E_{\mathrm{BY}}(y) & E_{\mathrm{AY}}(y) & 1 & E_{\mathrm{ZY}}(y) \\ 0 & 0 & 0 & 1 \end{bmatrix} \tag{A.14}$$

with

$$\chi := E_{\mathrm{C0Y}}\, y + E_{\mathrm{XY}}(y), \tag{A.15}$$

$$\delta := E_{\mathrm{YY}}(y) + E_{\mathrm{Y0Y}} + y, \tag{A.16}$$

and

$$\boldsymbol{T}^{y}_{z,real} = \begin{bmatrix} \boldsymbol{R}^{y}_{z}(z) & \boldsymbol{r}^{y}_{z} \\ \boldsymbol{0} & 1 \end{bmatrix} = \begin{bmatrix} 1 & -E_{\mathrm{CZ}}(z) & E_{\mathrm{BZ}}(z) & \delta \\ E_{\mathrm{CZ}}(z) & 1 & -E_{\mathrm{AZ}}(z) & \epsilon \\ -E_{\mathrm{BZ}}(z) & E_{\mathrm{AZ}}(z) & 1 & \phi \\ 0 & 0 & 0 & 1 \end{bmatrix} \tag{A.17}$$

with

$$\delta := E_{B0Z}z + E_{XZ}(z), \tag{A.18}$$

$$\epsilon := E_{A0Z}z + E_{YZ}(z), \tag{A.19}$$

$$\phi := E_{ZZ}(z) + E_{Z0Z} + z. \tag{A.20}$$

The real transformation matrix $\boldsymbol{T}^{t}_{w,real}$, which transforms from the workpiece to the tool coordinate system, results as follows:

$$\begin{aligned}\boldsymbol{T}^{t}_{w,real} =& \boldsymbol{T}^{t}_{z}\,\boldsymbol{T}^{z}_{y,real}\,\boldsymbol{T}^{y}_{x,real}\,\boldsymbol{T}^{x}_{r,real}\,\boldsymbol{T}^{r}_{w}\\ =& (\boldsymbol{T}^{z}_{t})^{-1}\,(\boldsymbol{T}^{y}_{z,real})^{-1}\,(\boldsymbol{T}^{x}_{y,real})^{-1}\\ & (\boldsymbol{T}^{r}_{x,real})^{-1}\,\boldsymbol{T}^{r}_{w}\\ =& \begin{bmatrix} 1 & \gamma & -\eta & \kappa\\ -\gamma & 1 & \iota & \lambda\\ \eta & -\iota & 1 & \mu\\ 0 & 0 & 0 & 1 \end{bmatrix}\end{aligned} \tag{A.21}$$

with

$$\gamma := E_{CX}(x) + E_{CY}(y) + E_{CZ}(z), \tag{A.22}$$

$$\eta := E_{BX}(x) - E_{BY}(y) - E_{BZ}(z), \tag{A.23}$$

$$\iota := E_{AX}(x) + E_{AY}(y) + E_{AZ}(z), \tag{A.24}$$

$$\begin{aligned}\kappa :=& - E_{B0Z}z - E_{BX}(x)w_z - E_{BY}(y)w_z\\ & - E_{BZ}(z)w_z + E_{BZ}(z)z - E_{C0Y}y\\ & + E_{CX}(x)w_y + E_{CY}(y)w_y - E_{CY}(y)y\\ & + E_{CZ}(z)w_y - E_{CZ}(z)y - E_{XX}(x)\\ & - E_{XY}(y) - E_{XZ}(z)\\ & - E_{X0X} + w_x - x,\end{aligned} \tag{A.25}$$

$$\begin{aligned}\lambda :=& - E_{A0Z}z + E_{AX}(x)w_z + E_{AY}(y)w_z\\ & + E_{AZ}(z)w_z - EAZ(z)z - ECX(x)w_x\\ & + E_{CX}(x)x - E_{CY}(y)w_x + E_{CY}(y)x\\ & - E_{CZ}(z)w_x + E_{CZ}(z)x - E_{YX}(x)\\ & - E_{YY}(y) - E_{YZ}(z)\\ & - E_{Y0Y} + w_y - y,\end{aligned} \tag{A.26}$$

$$\begin{aligned}\mu :=& - EAX(x)w_y - E_{AY}(y)w_y + E_{AY}(y)y\\ & - E_{AZ}(z)w_y + E_{AZ}(z)y + E_{BX}(x)w_x\\ & - E_{BX}(x)x + E_{BY}(y)w_x - E_{BY}(y)x\\ & + E_{BZ}(z)w_x - E_{BZ}(z)x - E_{ZX}(x)\\ & - E_{ZY}(y) - E_{ZZ}(z)\\ & - E_{Z0Z} - t_z + w_z - z.\end{aligned} \tag{A.27}$$

References

[1] Ramesh R, Mannan M, Poo A. Error compensation in machine tools — a review. Int J Mach Tools Manuf 2000;40(9):1235–56. http://dx.doi.org/10.1016/S0890-6955(00)00009-2.

[2] Weck M. Werkzeugmaschinen 5. Berlin, Heidelberg: Springer Berlin Heidelberg; 2006, http://dx.doi.org/10.1007/978-3-540-32951-0.

[3] Itō Y, editor. Thermal deformation in machine tools. New York, NY: McGraw-Hill; 2010.

[4] Mayr J, Jedrzejewski J, Uhlmann E, Alkan Donmez M, Knapp W, Härtig F, et al. Thermal issues in machine tools. CIRP Ann 2012;61(2):771–91. http://dx.doi.org/10.1016/j.cirp.2012.05.008.

[5] Brecher C, Spierling R, Fey M, Neus S. Direct measurement of thermo-elastic errors of a machine tool. CIRP Ann 2021;70(1):333–6. http://dx.doi.org/10.1016/j.cirp.2021.04.084.

[6] Wennemer M. Methode zur messtechnischen Analyse und Charakterisierung volumetrischer thermo-elastischer Verlagerungen von Werkzeugmaschinen [Ph.D. thesis], RWTH Aachen and IIF - Institut für Industriekommunikation und Fachmedien GmbH; 2018.

[7] Schwenke H, Knapp W, Haitjema H, Weckenmann A, Schmitt R, Delbressine F. Geometric error measurement and compensation of machines - An update. CIRP Ann 2008;57(2):660–75. http://dx.doi.org/10.1016/j.cirp.2008.09.008.

[8] Kwasny W, Turek P, Jedrzejewski J. Survey of machine tool error measuring methods. J Mach Eng 2011;11.

[9] Soichi Ibaraki, Wolfgang Knapp. Indirect measurement of volumetric accuracy for three-axis and five-axis machine tools: A review. IJAT 2012;6:110–24.

[10] ISO 230-3:2020. Test code for machine tools - part 3: Determination of thermal effects. 2020, ISO 230-3.

[11] Renishaw plc. Qc20-w wireless ballbar system. In: Renishaw plc, editor. 2013.

[12] Jindong Wang, Junjie Guo, Guoxiong Zhang, Bao Guo, Hongjian Wang. The technical method of geometric error measurement for multi-axis NC machine tool by laser tracker. Meas Sci Technol 2012;23(4):045003. http://dx.doi.org/10.1088/0957-0233/23/4/045003.

[13] Trapet E, Wäldele F. A reference object based method to determine the parametric error components of coordinate measuring machines and machine tools. Measurement 1991;9(1):17–22. http://dx.doi.org/10.1016/0263-2241(91)90022-I.

[14] Carmignato S, de Chiffre L, Bosse H, Leach RK, Balsamo A, Estler WT. Dimensional artefacts to achieve metrological traceability in advanced manufacturing. CIRP Ann 2020;69(2):693–716. http://dx.doi.org/10.1016/j.cirp.2020.05.009&domain=pdf.

[15] ISO 230-1:2012. Test code for machine tools - Part 1: Geometric accuracy of machines operating under no-load or quasi-static conditions. 2012, ISO 230-1.

[16] Viprey F, Nouira H, Lavernhe S, Tournier C. Novel multi-feature bar design for machine tools geometric errors identification. Precis Eng 2016;46:323–38. http://dx.doi.org/10.1016/j.precisioneng.2016.06.002.

[17] Liebrich T, Bringmann B, Knapp W. Calibration of a 3D-ball plate. Precis Eng 2009;33(1):1–6. http://dx.doi.org/10.1016/j.precisioneng.2008.02.003.

[18] Gomez-Acedo E, Olarra A, Orive J, La Lopez de Calle LN. Methodology for the design of a thermal distortion compensation for large machine tools based in state-space representation with Kalman filter. Int J Mach Tools Manuf 2013;75:100–8. http://dx.doi.org/10.1016/j.ijmachtools.2013.09.005.

[19] Kim K-D, Chung S-C. Synthesis of the 3D artefact for quick identification of thermal errors in machine tools. Int J Prod Res 2004;42(6):1167–87. http://dx.doi.org/10.1080/00207540310001614123.

[20] Kim K-D, Chung S-C. Synthesis of the measurement system on the machine tool. Int J Prod Res 2001;39(11):2475–97. http://dx.doi.org/10.1080/00207540110045939.

[21] Yang M, Lee J. Measurement and prediction of thermal errors of a CNC machining center using two spherical balls. J Mater Process Technol 1998;75(1–3):180–9. http://dx.doi.org/10.1016/S0924-0136(97)00316-6.

[22] Chen J-S. Fast calibration and modeling of thermally-induced machine tool errors in real machining. Int J Mach Tools Manuf 1997;37(2):159–69. http://dx.doi.org/10.1016/S0890-6955(96)00042-9.

[23] Breitzke A, Hintze W. Workshop-suited geometric errors identification of three-axis machine tools using on-machine measurement for long term precision assurance. Precis Eng 2022;75:235–47. http://dx.doi.org/10.1016/j.precisioneng.2022.02.006.

[24] Sartori S, Zhang GX. Geometric error measurement and compensation of machines. CIRP Ann 1995;44(2):599–609. http://dx.doi.org/10.1016/S0007-8506(07)60507-1.

[25] Bringmann B. Improving geometric calibration methods for multi-axis machining centers by examining error interdependencies effects [Ph.D. thesis], ETH Zurich; 2007, http://dx.doi.org/10.3929/ethz-a-005424013.

[26] Zhu S, Ding G, Qin S, Lei J, Li Zhuang, Yan K. Integrated geometric error modeling, identification and compensation of CNC machine tools. Int J Mach Tools Manuf 2012;52(1):24–9. http://dx.doi.org/10.1016/j.ijmachtools.2011.08.011.

[27] Zhang G, Veale R, Charlton T, Borchardt B, Hocken R. Error compensation of coordinate measuring machines. CIRP Ann 1985;34(1):445–8. http://dx.doi.org/10.1016/S0007-8506(07)61808-3.

[28] Donmez MA, Blomquist DS, Hocken RJ, Liu CR, Barash MM. A general methodology for machine tool accuracy enhancement by error compensation. Precis Eng 1986;8(4):187–96. http://dx.doi.org/10.1016/0141-6359(86)90059-0.

[29] Kurtoglu A, Sohlenius G. The accuracy improvement of machine tools. CIRP Ann 1990;39(1):417–9. http://dx.doi.org/10.1016/S0007-8506(07)61086-5.

[30] Soons JA, Theuws FC, Schellekens PH. Modeling the errors of multi-axis machines: a general methodology. Precis Eng 1992;14(1):5–19. http://dx.doi.org/10.1016/0141-6359(92)90137-L.

[31] Kreng VB, Liu CR, Chu CN. A kinematic model for machine tool accuracy characterisation. Int J Adv Manuf Technol 1994;9(2):79–86. http://dx.doi.org/10.1007/BF01750414.

[32] Kiridena V, Ferreira PM. Kinematic modeling of quasistatic errors of three-axis machining centers. Int J Mach Tools Manuf 1994;34(1):85–100. http://dx.doi.org/10.1016/0890-6955(94)90042-6.

[33] Chen XB, Geddam A, Yuan ZJ. Accuracy improvement of three-axis CNC machining centers by quasi-static error compensation. J Manuf Syst 1997;16(5):323–36. http://dx.doi.org/10.1016/S0278-6125(97)88463-4.

[34] Yang J, Altintas Y. Generalized kinematics of five-axis serial machines with non-singular tool path generation. Int J Mach Tools Manuf 2013;75:119–32. http://dx.doi.org/10.1016/j.ijmachtools.2013.09.002.

[35] Soori M, Arezoo B, Habibi M. Virtual machining considering dimensional, geometrical and tool deflection errors in three-axis CNC milling machines. J Manuf Syst 2014;33(4):498–507. http://dx.doi.org/10.1016/j.jmsy.2014.04.007.
[36] Tian W, Gao W, Chang W, Nie Y. Error modeling and sensitivity analysis of a five-axis machine tool. Math Probl Eng 2014;2014:1–8. http://dx.doi.org/10.1155/2014/745250.
[37] Cong DC, Chinh BB, Jooho H. Volumetric error model for multi-axis machine tools. Procedia Manuf 2015;1:1–11. http://dx.doi.org/10.1016/j.promfg.2015.09.023.
[38] Pan F, Nie L, Bai Y, Wang X, Liu K, Wu X. Error compensation for coordinate measuring machine. IOP Conf Ser Mater Sci Eng 2018;394:032068. http://dx.doi.org/10.1088/1757-899X/394/3/032068.
[39] Globke W. Koordinaten, transformationen und roboter. Karlsruhe; 2015.
[40] ISO 10360-2:2009. Geometrical product specifications (GPS) - acceptance and reverification tests for coordinate measuring machines (CMM) - part 2: CMMs used for measuring linear dimensions. 2009, ISO 10360-2:2009.
[41] Kunzmann H, Trapet E, Wäldele F. A uniform concept for calibration, acceptance test, and periodic inspection of coordinate measuring machines using reference objects. CIRP Ann 1990;39(1):561–4. http://dx.doi.org/10.1016/S0007-8506(07)61119-6.
[42] Trapet E, Wäldele F. A reference object based method to determine the parametric error components of coordinate measuring machines and machine tools. Measurement 1991;9(1):17–22. http://dx.doi.org/10.1016/0263-2241(91)90022-I.
[43] Lee ES, Burdekin M. A hole-plate artifact design for the volumetric error calibration of CMM. Int J Adv Manuf Technol 2001;17(7):508–15. http://dx.doi.org/10.1007/s001700170151.
[44] Miura Y, Nakanishi S, Higuchi E, Takamasu K, Abe M, Sato O. Comparative evaluation of estimation of hole plate measurement uncertainty via Monte Carlo simulation. Precis Eng 2019;56:496–505. http://dx.doi.org/10.1016/j.precisioneng.2019.02.007.
[45] SEW 385:1991. Iron alloys with special thermal extension. 1991, SEW 385:1991.
[46] Pfeiffer D. Kompensation thermisch bedingter Bearbeitungsfehler durch prozeßnahe Qualitätsregelung. ISW Forschung und Praxis, Berichte aus dem Institut für Steuerungstechnik der Werkzeugmaschinen und Fertigungseinrichtungen der Universität Stuttgart, vol. 72, Berlin and Heidelberg: Springer; 1988, http://dx.doi.org/10.1007/978-3-662-08148-8.
[47] Ibaraki S, Knapp W. Indirect measurement of volumetric accuracy for three-axis and five-axis machine tools: A review. Int J Autom Technol 2012;2012(6):110–24. http://dx.doi.org/10.3929/ethz-a-007593181.
[48] Viprey F, Nouira H, Lavernhe S, Tournier C. Modelling and characterisation of geometric errors on 5-axis machine-tool. Mech Ind 2019;20(6):605. http://dx.doi.org/10.1051/meca/2019034.
[49] ISO/IEC Guide 98-3:2008. Uncertainty of measurement - part 3: Guide to the expression of uncertainty in measurement (GUM:1995). 2008, ISO/IEC Guide 98-3.
[50] ISO/IEC Guide 99:2007. International vocabulary of metrology - basic and general concepts and associated terms (VIM). 2007, ISO/IEC Guide 99.
[51] Renishaw GmbH. Datenblatt OMP400. 2016.
[52] ISO/TR 230-9:2005. Test code for machine tools - part 9: Estimation of measurement uncertainty for machine tool tests according to series ISO 230, basic equations. 2005, ISO/TR 230-9.